10

Optical Measurements: Polarization and Coherence of Light Fields

O. V. Angelsky[1], P. V. Polyanskii[1], I. I. Mokhun[1],
C. Yu. Zenkova[1], H. V. Bogatyryova[2], Ch. V. Felde[1],
V. T. Bachinskiy[3], T. M. Boichuk[3] and A. G. Ushenko[1]
[1]*Chernivtsi National University, Chernivtsi,*
[2]*National Technical University of Ukraine "Kiev Polytechnic Institute", Kiev,*
[3]*Bukovonian State Medical University, Chernivtsi,*
Ukraine

1. Introduction

The Chapter is devoted to consideration of metrological aspects of intrinsically interconnected characteristics of light fields, such as intensity, polarization and coherence. Conceptually, all these quantities are derived from the Wolf's coherency matrix [1]. However, new insight on interconnection of them is provided by the novel singular-optical approach [2, 3] predicting existence of important regularities in electromagnetic fields which were early considered as quite random ones. So, phase singularities of scalar (homogeneously polarized), polarization singularities of vector (inhomogeneously polarized) fields, as well as singularities of correlation functions of partially coherent, partially polarized fields constitute specific skeletons, i.e. "bearing" elements of a field. Knowing the loci and characteristics of such elements, one can judge on behavior of a field at its other areas, at least in qualitative manner, but quite reliably [4]. This circumstance opens quite new possibilities for metrology of optical fields and leads to prospective practical applications of new metrological techniques.

We discuss here interconnections of polarization and coherence characteristics of light fields in various manifestations of them, both as one-point and two-point functions. For that, in development of earlier approaches, we show the framework for generalization of polarization metrology on a wide class of combined optical beams assembled as mutually incoherent (or partially mutually coherent) components, which can be orthogonal in polarization. Such generalization provides taking into account partial polarization and associated vector singularities, which can be used in non-destructive optical diagnostics as well as in optical telecommunications with polarization coding.

Further, we represent point-by-point Stokes-polarimetric technique and singular-optical concept of polarization diagnostics. Feasibilities of combined application of conventional interferometry and local Stokes-polarimetry are substantiated.

Important part of this review is devoted to description of feasibilities for experimental measuring of coherence by measuring of spatial polarization distributions of

inhomogeneously polarized fields. We represent the newest metrological tool connected with novel concept of optical currents (optical flows). Namely, we show that some intimate characteristics of complex optical fields with arbitrary degree of spatial coherence and arbitrary degree of polarization may be "deciphered" indirectly, by observation of the influence of such fields on embedded micto- and nanoparticles. This original metrological approach seems to be prospective for development of so-called optical traps and tweezers for manipulation of isolated particles of micro- and nanoscales.

Separate section of the Chapter is devoted to application of local Stokes-polarimetry in diagnostics of biological tissues, in the context of early (pre-clinical) diagnostics of some widespread diseases. We represent both experimental and data processing techniques leading to high-sensitive and reliable diagnostics.

All considered metrological approaches and techniques are original, generated by recently by the members of our team.

Some prospects of further investigations in the direction represented in this Chapter, as well as necessity and possible ways for overcoming some present shortcomings of optical metrology in the field of coherence and polarization, are outlined in the last section.

2. Historical outlook

The notion of coherence is the most fundamental concept of modern optics. As it has been shown by E. Wolf [5], this notion is intrinsically connected with other characteristics of light, such as intensity and polarization. One can distinguish between these characteristics mainly in didactic purposes. But in every practically important case we meet the problem of tight, inseparable interconnection of them. So, one cannot define coherence, in part aspiring to associate it with visibility of interference pattern, ignoring for that the states of polarization of superposed beams. Note, that attempts to explain the Young's interference experiment for "completely unpolarized" light lead sometimes to questionable conclusions [6]. At the same time, the most fundamental definition of polarized light is given just through the measure of mutual coherence of the orthogonally polarized components of a beam. At last, all three mentioned characteristics of a light beam are comprehensively expressed through known combinations of the Wolf's coherency matrix elements [1].

Incidentally, urge towards to associate coherence just with obvious interference (intensity modulation) effect does not always lead to true understanding the coherence phenomena. It is not enough that interference fringes are absent in superposition of completely mutually coherent but orthogonally polarized beams (it is well-known from the Fresnel-Arago laws and experiments). There are quite new concepts showing the absence of interference effect for superposing two waves of equal frequencies with strictly (*deterministically*) connected complex disturbances even with the same state of polarization. Refined example of this kind was given by L. Mandel in his concept of "anticoherence" [7]. In very simplified form, the Mandel's concept can be formulated in terms of conventional (static) holography.

As it is well known, a simple thin hologram reconstructs in plus-minus first diffraction orders two conjugate fields producing so-called main and conjugate images [8]. Having reliable techniques for optical phase conjugation, one can try to add two complex conjugated copies of the signal at one plane, to say at a plane of hologram. What is the result? Intensity of superposition of two such waves is determined as

$$I = < \left| a \exp\left[i\left(\omega t - \mathbf{kr} + \varphi_1\right)\right] + b \exp\left[-i\left(\omega t - \mathbf{kr} + \varphi_2\right)\right] \right|^2 > , \quad (1)$$

where a and b are amplitudes of two conjugated waves that are believed constants (stationary optical fields [9]), $\omega = 2\pi/T$ is angular frequency of oscillations (T being a time period) that is the same for both superposed counterparts, $\mathbf{k}$ is the wave vector, $\mathbf{r}$ is the position vector of the observation point, $\varphi_{1,2}$ are the initial phases of two waves, and $< ... >$ denotes time averaging. It is easy to see that, in contrast with common interference, the temporal multiplier does not vanish in this expression:

$$I = a^2 + b^2 + 2ab < \cos\left[2\left(\omega t - \mathbf{kr}\right) + \left(\varphi_1 - \varphi_2\right)\right] > \equiv a^2 + b^2 , \quad (2)$$

so that the averaging results in vanishing the "interference" term. This conclusion is illustrated in Fig. 1, from which one can see that summation of two complex conjugated beams, u and u^*, everywhere along the Arrow of time gives rise to the real value of constant magnitude. Thus, interference between deterministically, unambiguously connected two waves of equal frequency and identical state of polarization is absent. Of course, if one implements phase conjugation of one of two waves figuring in Eq. (1), interference effect will be provided due to compensation of the temporal multiplier and, as a consequence, inefficiency of time averaging.

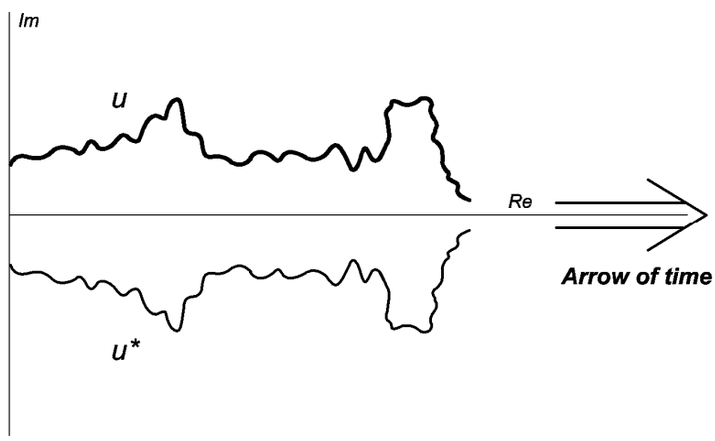

Fig. 1. Superposition of two complex conjugated replicas of a signal results in a real signal of constant amplitude along the Arrow of time, without interference effect.

What is less discussed within the framework of classical (wave) theory of partial coherence is the influence of an "observer" on coherent properties of studied beams. This problem is quite typical for quantum optics [10 - 12] (as well as for quantum physics in general [13]). But the results obtained along last quarter of a century compel to take into account influence of the conditions of observation and detector characteristics on evaluation of the coherence of light in classical approach also. Let us give some arguments for this point.

When we consider interference of two waves with close but non-equal frequencies ($\omega_1 \neq \omega_2$, $\Delta\omega << \bar{\omega}$), we observe moving intensity fringes. This effect is widely used in the optical

heterodyning (optical nonlinear mixing) technique. If the "register" is stationary and possesses low temporal resolution, averaging over large enough temporal interval results in smoothing of interference fringes, so that visibility $V \to 0$; we conclude that two waves are mutually incoherent. But, on the other hand, using a "register" with higher temporal resolution, which moves in the direction and with speed of propagation of moving intensity waves, we recognize the same two waves as mutually coherent that *form* observable interference fringes in moving coordinates! To say, one can register a hologram form such waves at the properly moving "register" (though this task is not simple in practice).

Once more example related to the problem of interest is the influence of *spectral* resolution (or, more strictly, inhomogeneous spectral sensitivity) of the detector on our conclusions concerning *spatial* coherence of the elaborated optical field. If one uses in the classical Young's two-pinhole interference arrangement a source with uniform spectral density, then a detector with uniform spectral sensitivity "evaluates" the field as completely spatially incoherent for arbitrary sampling points at the beam cross-section due to superposing numerous scaled in wavelength spectral interference patterns, so that minima of intensity (of the field of homogeneous spectral distribution!) are absent in the resulting pattern. *Such detector is "blind" to spatial coherence of such optical field*. Nevertheless, the human eye detects spatial coherence of a field due to non-uniform spectral sensitivity of visual receptors and inhomogeneous spatial distribution of *colors* over analyzed field. Of course, the same is true for evaluation of *temporal* coherence, to say, in the arrangement of the Newton's rings in white light.

Less trivial case has been considered by Wolf [14, 15, see also numerous useful references herein] in the context of induced spectral changes resulting in remarkable transformations of temporal coherence of polychromatic optical fields due to the presence of material *intermediary*, as diffraction or scattering object.

The next, and more closer to our consideration, example – *pseudodepolarization* [16] (in modern terminology, "global" depolarization [6]) resulting from stationary scattering of laser radiation in multiply scattering media, such as turbid media, multi-mode waveguides, the most of natural objects, including biological ones. Here the role of detector becomes fundamental. Really, the universal approach to determine all polarization characteristics of a field (both the state of polarization and the degree of polarization [17]) consists in Stokes-polarimetry of the analyzed field. For that, Stokes-polarimetric analysis gives quite different results for local and "global" (space-averaged) measurements. So, the point-wise measuring Stokes parameters shows complete (unity) degree of polarization, but the state of polarization changes from point to point. Space averaging over ten and more speckles shows seeming depolarization. This case is the central subject of study of vector singular optics [18].

The mentioned examples illustrate, in part, importance of taking into account of temporal and spatial resolution of the used detector, as well as a choice of the coordinates (stationary or moving) for metrological estimation of coherence and polarization of light, and even understanding (*definition*) of these phenomena.

Let us briefly highlight another two positions that are important for our consideration. Firstly, as it has been pointed out by I. Freund [19], we do not ready to investigate experimentally the problem of coherence and polarization of optical light in general, 3D

case, when paraxial approximation violates and one cannot neglect any of three Cartesian coordinates for description of behaviour of the electric vector. As an example, Freund references the study of polarization of relict – cosmic microwave radiation (CMR) [20] that is believed to be almost *isotropic* (nondirectional) [21]. Measuring the Stokes parameters for such radiation is, to all appearance, not well-grounded. It is the same that measuring the Stokes parameters in various directions from interior of a cloud of light-scattering small particles, what approach is not generally accepted [22, 23]. Nevertheless, it is the only what we have!

The second example concerns directly to one of the problem discussed in the following sections of this overview, *viz.* so-called *optical currents (flows)* [24]. Though it is prematurely now to solve comprehensively this problem, especially in experimental aspect, it is clear that micro- or nanoparticles serving for diagnostics of inhomogeneously polarized and partially coherent optical field [25 - 30] affect this field as absorbing and retransmitting particles with their own characteristics, so that the state of a field, in general, changes under influence of such secondary radiators.

Pronouncing call of the times in the topic under consideration consists in involving the ideas, approaches and techniques of Singular Optics [2]. It is seen, in part, from recent important review [3] devoted to the structure of partially coherent optical fields. Investigations in this scientific domain have been actually stimulated, in part, by papers [31 - 34]. For that, many usual and new results of the theory of partial coherence and partial polarization become essentially urgent just in the singular optics concept. On the other hand, there are good reasons to wait that attracting the fundamentals of the theory of partial coherence will lead to development of new practical applications of singular optics. So, two mentioned areas are of "mutual benefits".

Moreover, as it has been argued in papers [30, 35, 36], "*Usual beam parameters either characterize a beam 'in a whole' (power, momentum, beam size and divergence angle) or describe its 'shape' via certain spatial distributions (amplitude, phase, polarization state, etc.)… Usual beam parameters provide only rough and, sometimes, distorted picture of internal processes that constitute a real 'inner life' of a light beam. These processes are related to the fundamental dynamical and geometrical aspects of light fields, and are associated with the permanent energy redistribution inside the beam 'body', which underlies the beam evolution and transformations. The internal energy flows provide a natural and efficient way for 'peering' into the light fields and studying their most intimate and deep features.*" It is of interest, in the context of this review, to correlate this statement with the Wolf's methodology of observable quantities that is the most influential concept of physical optics since 1954: "optics of observable quantities, such as correlation functions and averaged in time intensities" [17]. Paradoxial contradiction between two undoubtedly true statements is apparent. Really, this contradiction is just eliminated as one takes into account that internal energy flows ("optical currents" [24]) may be revealed only by carrying out the experiments with observable quantities. Similarly, vibrational phase [18] of an optical wave is unobservable, while its difference with a phase of coherent reference phase is liable to registration just as the phase of the mutual coherence function of two waves. More globally, two mentioned approaches are complementary, being intimately interconnected, similarly to approaches of statistical physics and thermodynamics.

To facilitate understanding the material of the following sections, let us briefly remind the main light beam characteristics involved in our consideration. The key notion of *geometrical optics* is a ray; a bundle of rays constitutes an optical beam. The only information provided by rays is the direction of propagation of light. More diverse, more fundamental and more informative parameters of light are derived within the framework of wave optics. There are wave amplitude and phase (both quantities are unobservable directly though lying in the basis of theory [17]); polarization that is determined by the amplitude ratio and phase difference of orthogonal components of a beam; the degree of polarization is determined by correlations between these components; coherence parameters characterizing concordance of light disturbances at two (or more) spatial-temporal points of light field. These base characteristics defined in seminal book [17] as well as in numerous other handbooks in optics, are added by the Poynting vector determining the direction of propagation of light beams in terms of electrodynamics, and by more complex polarization parameters than simple azimuth of polarization and ellipticity inherent in elementary wave optics. In our study, much attention will be paid to the Stokes parameters, polarization parameters intrinsically connected with both energy and coherent characteristics of light beams. These notions will be specified in the corresponding sections of the chapter.

Organization of the review is not quite usual. The most of review papers written up to now on the topic of interest are of theoretical nature, sometimes with valued simulation background. Relatively less attention is paid to experimental aspects of the problem. Partially, this gap is filled by recent books and book chapters written by the authors of this review [37, 38]. But the scope of experimental results rapidly grows, and this outlook does not repeat our previous papers. So, we represent here several independent experimental current views on the problem of metrology of coherent and polarization properties of optical fields, with especial accent on singular optical prerequisites and consequences of our experimental approaches. In spite of forced incompleteness of this consideration, the authors hope that it would stimulate further experimental investigations in this field and lead to broadening of practically significant applications of *Singular Optics of Partially Coherent and Inhomogeneously Polarized Optical Fields*.

3. Investigation of optical currents in completely coherent and partially coherent vector fields

In this section we present the computer simulation results on the spatial distribution of the Poynting vector and illustrate motion of micro and nanoparticles in spatially inhomogeneously polarized fields.

The Poynting vector $\mathbf{S}$, is defined, in its simplest form, as the vector product of the vectors of electric field, $\mathbf{E}$, and magnetic field, *viz.* $\mathbf{H}$, $\mathbf{S} = \mathbf{E} \times \mathbf{H}$. This form is referred to as the Abraham form of the Poynting vector. By definition, the Pointing vector *for a plane wave* is perpendicular to vectors $\mathbf{E}$ and $\mathbf{H}$, being representing the energy flux (in W/m^2) of an electromagnetic field. As it will be seen from the following consideration, in light fields with complex wave fronts and with variable in space (inhomogeneous) state of polarization the Poynting vector can exhibit much more sophisticated behavior, being also changing from point to point at the beam cross-section and leading to new applications of light.

The use of small particles for diagnostics of microstructure of light is widely used approach [25 - 30], but mainly in approximation of complete coherence of an optical field. Here, the influence of phase relations and the degree of mutual coherence of superposing waves in two-wave and four-wave configurations on the characteristics of the microparticle's motion is analyzed. The possibility of diagnostics of optical currents in liquids caused by polarization characteristics of an optical field alone is demonstrated using nanoscale metallic particles. We also discuss the prospects of studying temporal coherence using the proposed approach.

There is the motivation of this study. Experimental investigation and computer simulation of the behavior of small spherical particles embedded in optical fields provide a deeper understanding of the role of the Poynting vector for description of optical currents in various media [24, 36]. So, interference between waves polarized in the plane of incidence has been shown to be effective in creation of polarization micro-manipulators and optical tweezers. On the other hand, this is a vital step in optimal metrological investigation of optical currents in vector fields [39 - 42]. Besides, the study of spatial and temporal peculiarities of the motion of particles embedded in optical fields with various spatial configurations and with various scale distributions of the Poynting vector leads to new techniques for estimating the temporal coherence of optical fields [43].

Computation of the spatial distribution of the time-averaged Poynting vector determining the forces affecting microparticles and their movement is performed following the algorithm proposed by M. Berry [24] who has shown that the vector force affecting a small particle in an optical field is proportional to the time-averaged Poynting vector. We will show that the study of the motion of microparticles in inhomogeneously polarized fields provides reconstruction of the spatial distribution of the time-averaged Poynting vectors, *viz.* the optical currents.

3.1 Two-wave superposition for changeable degree of mutual coherence of the components

Superposition of two plane waves of equal amplitudes polarized in the plane of incidence (Fig. 2a) results in the distribution of the Poynting vector shown in Fig. 2b. Such distribution arises when the interference angle is equal to 90°, and the only periodical polarization modulation of the field (in the absence of intensity modulation) takes place in the plane of observation [44].

The coherency matrix $W(\mathbf{r}_1,\mathbf{r}_2,t)$ describes the coherence properties of vector optical fields, being characterising the correlation of two fields at two different spatial points $\mathbf{r}_1$ and $\mathbf{r}_2$ [45, 46], and is determined as

$$W(\mathbf{r}_1,\mathbf{r}_2,t) = < E^{(1)}{}_i(\mathbf{r}_1,t)E_j^{(2)*}(\mathbf{r}_2,t) >$$

where $i, j = x, z$. Within the framework of such approach the degree of mutual coherence of the field is defined as [15]

$$\eta_{ij}(\mathbf{r}_1,\mathbf{r}_2,t) = \frac{W_{ij}(\mathbf{r}_1,\mathbf{r}_2,t)}{\sqrt{\mathrm{tr}[W(\mathbf{r}_1,\mathbf{r}_1,0)]\cdot\sqrt{\mathrm{tr}[W(\mathbf{r}_2,\mathbf{r}_2,0)]}} = \frac{W_{ij}(\mathbf{r}_1,\mathbf{r}_2,t)}{\sqrt{\sum_{ij} W_{ii}(\mathbf{r}_1,\mathbf{r}_1,0)W_{jj}(\mathbf{r}_2,\mathbf{r}_2,0)}} \quad (3)$$

The distribution of the time-averaged density of the energy current in space determines the current magnitude at different points of the plane of observation, being unambiguously determined by the degree of coherence of the superposing waves. The direction of the resulting current is set by the directions of the Poynting vectors of these waves.

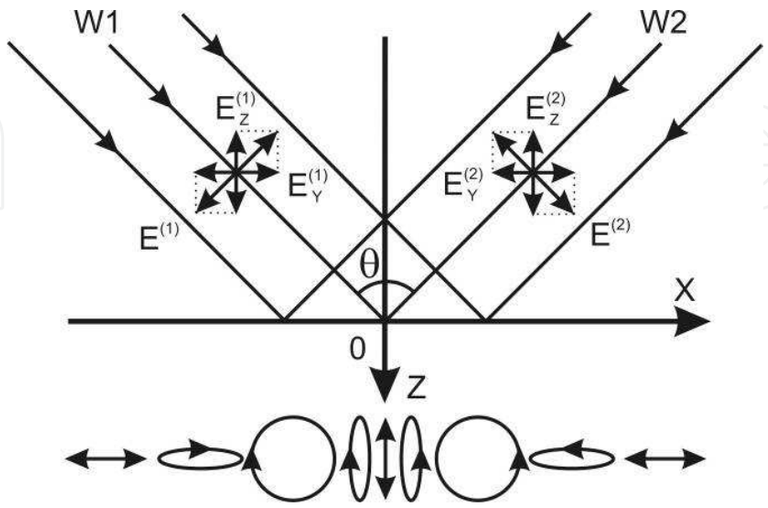

Fig. 2a. Superposition of plane waves of equal amplitudes linearly polarized in the plane of incidence having an interference angle of 90°. Periodical spatial polarization modulation takes place in the plane of incidence.

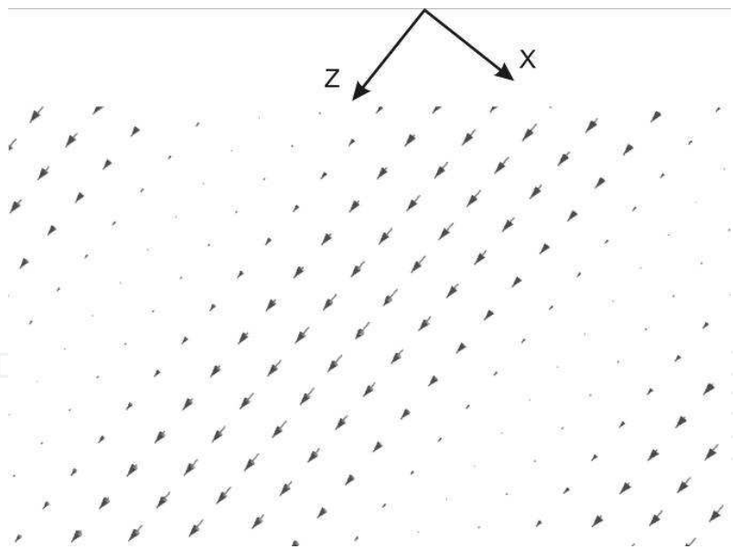

Fig. 2b. Spatial distribution of the time-averaged Poynting vectors resulting from superposition of two orthogonally linearly polarized waves with an interference angle of 90°.

An analysis of the spatial distribution of the time-averaged Poynting vectors shown in Fig. 2b reveals the periodicity of this distribution, where the lengths of lines shown in the figure are proportional to the absolute magnitudes of the vectors. The lines corresponding to the singularities of the Poynting vector are shown by the indicated set of points [47 - 49].

Spatial distribution of the time-averaged Poynting vectors, cf. Fig. 2b, shows the trajectories of energy transfer. The points at the map of the time-averaged Poynting vectors (Fig. 2b) correspond to the areas through which energy transfer is absent, showing: (i) the loci of singularities of the Poynting vector; (ii) the points (with constant intensity) forming the directions along which light energy is non-vanishing, but is conserved; (iii) the points where the vector H vanishes due to interference, while in this arrangement (90°-superposition of plane waves) superposition of strictly coaxial vectors H of equal amplitudes associated with two superimposed plane waves takes place.

On the other hand, the instantaneous magnitude of the electric (magnetic) field strength's vector of the resulting distribution, which is formed in the plane of observation, is written as

$$\mathbf{E} = \left|\mathbf{E}^{(1)} + \mathbf{E}^{(2)}\right| \cos(\omega t + \delta_e)\mathbf{a}_e \quad (\text{or } \mathbf{H} = \left|\mathbf{H}^{(1)} + \mathbf{H}^{(2)}\right| \cos(\omega t + \delta_h)\mathbf{a}_h),$$

where, $\mathbf{a}_e$, $\mathbf{a}_h$ are the unit vectors in the direction of propagation of the electric (magnetic) components for the resulting field in the plane of observation; δ_e (δ_h) is the phase difference of the electric (magnetic) field components of superposed waves. In this case, the instantaneous magnitude of the Poynting vector is

$$\mathbf{S}_{inst} = \mathbf{E} \times \mathbf{H} = |\mathbf{E}| \cdot |\mathbf{H}| \cos(\omega t + \delta_e) \cos(\omega t + \delta_h)(\mathbf{a}_e \times \mathbf{a}_h),$$

and the time-averaged magnitude of the Poynting vector is

$$\mathbf{S}_{ave} = \frac{|\mathbf{E}| \cdot |\mathbf{H}|}{2}(\mathbf{a}_e \times \mathbf{a}_h)\cos(\delta_e - \delta_h) = \frac{1}{2}(\mathbf{E} \times \mathbf{H}) \cdot \cos(\delta_e - \delta_h). \quad (4)$$

Because the phase difference of the electric field changes from point to point (polarization modulation), the time-averaged magnitude of the Poynting vector is modulated in space taking the maximum (minimum) at different points of the plane of observation, as it is seen from Eq. (4).

Homogeneous intensity distribution and periodical spatial modulation of the Poynting vector simultaneously realized in the observation region have previously been discussed within the framework of Refs [50, 51]. Spatial polarization modulation at the plane of observation is caused by superposition of the E_x and E_z field components with changing the phase difference from point to point, cf. Fig. 2a. A photodetector registers only intensity, $I = E_x^2 + E_z^2$. The sum of the squared amplitudes of the electrical field components is constant at the plane of observation, though the state of polarization changes. The Poynting vector is defined, as mentioned above, by the vector product, $S = E \times H$. One observes the dependence of the result on the phase relation between vectors **E** and **H** through the vector magnitude and its direction. This relation changes from point to point in the plane of observation and manifests itself in polarization modulation. An obvious explanation for this follows from consideration of the vector product of the components of vector **E** (E_x and E_z components) with vector **H**. Both the magnitudes of projections E_x and E_z and their phases change from point to point in the observation plane. As a consequence, the vector product changes as well as the Poynting vector. The result of modulation is shown in Fig. 3.

The results of simulating the motion of particles embedded in the field of the considered distribution of the Poynting vector are shown in Fig. 4. We have here tacitly assumed the particles to be absorbing and of size 0.1 μm. One observes that in the case of the distribution resulting from superposition of completely mutually coherent waves, the velocities of particle motion along the lines of maxima and zeroes of the Poynting vector are considerably different from one another.

The particle size is here comparable with a half-period of the corresponding distribution; however, the resultant force giving rise to the particle motion along the lines close to the Poynting vector maxima exceeds the resultant force for lines close to the zeroes of the Poynting vector. The results of modulation of particle movement velocity along the peaks and zeroes of the averaged field of the Poynting vector are shown in Fig. 4a and Fig. 4b, respectively.

If the degree of mutual coherence of the superposed waves equals 0.2, the spatial distribution of the averaged Poynting vectors becomes more homogeneous, the modulation depth decreases considerably, and the velocities of microparticles become almost identical.

When the degree of mutual coherence equals 0.5, the relative velocities of the microparticles along the same trajectories are lower in comparison with velocities in case of complete mutual coherence of the superposed waves and lie in the vicinity of the average magnitudes for coherent and incoherent cases [52]. One observes the dependence on the coherent properties of the superimposed waves for the motion velocities of microparticles with constant size and form in media with constant viscosity [52]. When analyzing the motion of test particles in the region of distributed magnitude of the Poynting vector, the influence of the parameters of superposing fields on the character of particle motion can be determined, cf. Fig. 4a, 4b.

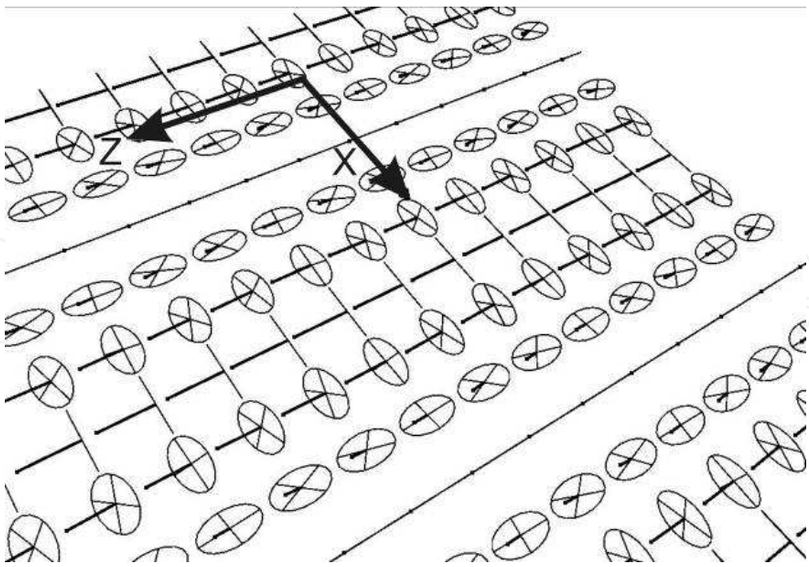

Fig. 3. The polarization distribution in the registration plane is marked by thin lines. The direction and magnitude of the Poynting vector are marked by bold lines. The point at the end of the vector determines the energy transfer direction. The modulation of the Poynting vector takes place according to the polarization modulation at the plane of observation.

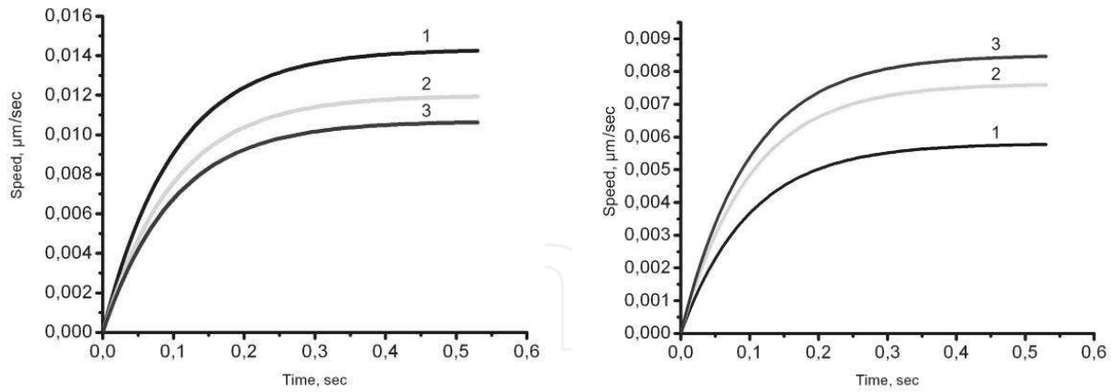

a b

Fig. 4. The change of the particle motion velocity with time obtained for different magnitudes of the degree of coherence of superposing waves in the case of particles moving along the peak (*a*) and the minimum (*b*) of the field of time-averaged Poynting vector magnitude: curves 1, 2, and 3 correspond to the degree of coherence, which equals 1, 0.5, and 0.25, respectively.

When the degree of mutual coherence equals 0.5, the relative velocities of the microparticles along the same trajectories are lower in comparison with velocities in case of complete mutual coherence of the superposed waves and lie in the vicinity of the average magnitudes for coherent and incoherent cases [52]. One observes the dependence on the coherent properties of the superimposed waves for the motion velocities of microparticles with constant size and form in media with constant viscosity [52]. When analyzing the motion of test particles in the region of distributed magnitude of the Poynting vector, the influence of the parameters of superposing fields on the character of particle motion can be determined, cf. Fig. 4a, 4b.

As it was shown in papers [44, 51, 52], the degree of coherence of superposing waves determines not only the visibility of an interference distribution, but also the structure of the polarization field, *viz.* it determines the distribution of the Poynting vector. Under the same other conditions of the wave superposition, *changing the degree of coherence results in changing motion velocity of the test particles, what can serve as an estimating parameter for determining the coherence properties of superposing waves*. These differences in velocities of motion of microparticles are explained physically in the following manner: Increasing the share of incoherent radiation in the resulting field distribution causes a decrease of the modulation depth of the Poynting vector's spatial distribution, as well as a decrease of the resultant force magnitude along the lines of energy transfer, which induces the motion of the microparticles. The increase of the degree of coherence brings about an accelerated particle motion in the field of averaged energy magnitudes.

The following diagram (Fig. 5) shows the particle velocity distribution (in this case, 39 particles), embedded into the field formed by the averaged magnitudes of the Poynting vector in the case of superposition of completely mutually coherent waves. With time (~1.2 sec) practically all particles gain equal velocity magnitudes (see column 7); redistribution of particles in the direction of the resultant force and uniform motion along the zero value of the Poynting vector take place.

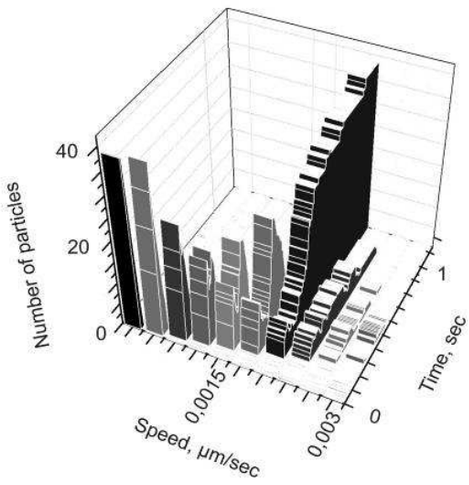

Fig. 5. The diagram of particles velocity distribution with time.

3.2 Superposition of four waves for changeable degree of mutual coherence of the components

In the case of superposition of four waves, see Fig. 6a, involving two sets of counter-propagating plane waves of equal intensities, linearly polarized in the plane of incidence and oriented at an angle of 90° with respect to each other, the spatial distribution of the time-averaged Poynting vectors is formed as shown in Fig. 6b.

The 2D periodicity of the Poynting vector's distribution is evident. As in the previous case, the lengths of the time-averaged Poynting vectors are proportional to their magnitudes. The nodal points in this distribution correspond to zero magnitudes of the Poynting vector, i.e. singularities of the Poynting vector. In the following simulation, the diameters of the particles are changed to be comparable with a half-period of the corresponding spatial distribution of the Poynting vector.

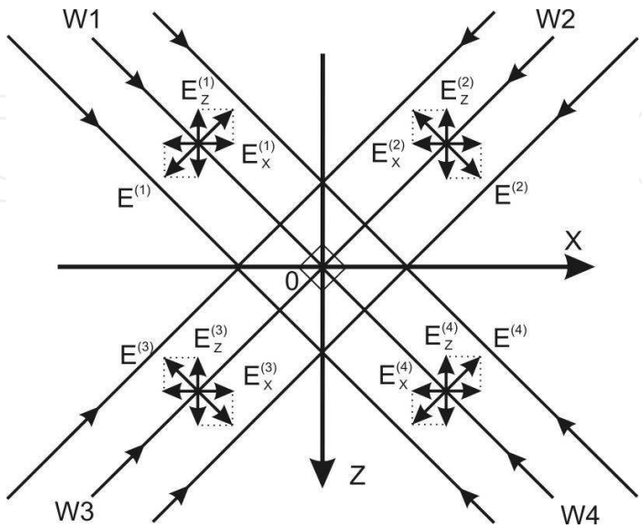

Fig. 6a. Arrangement of superposition of four plane waves.

This follows from the presence of the minimum of the modulation depth at the spatial distribution of the Poynting vector. If the phase relations between four superposed beams are such that the modulation depth of the spatial distribution of the Poynting vector is maximal, the particle velocities will depend on the degree of mutual coherence between the interfering beams, see Fig. 7.

In order to compare the influence of the temporal and spatial parameters of coherence on the motion of the microparticles, we have analyzed the maps of the time-averaged Poynting vector with a superposition of four plane waves over a large area. During this, we have tracked the microparticles' motion. The dependence of microparticles' velocities on the phase difference of the superposing beams has thus been revealed. So, in the case of pair-by-pair four opposite-in-phase superposed beams, particles become motionless. For that, the "opposite-in-phase" configuration covers the situation where two sets of mutually orthogonal standing waves are characterized by the fact that their nodes strictly coincide.

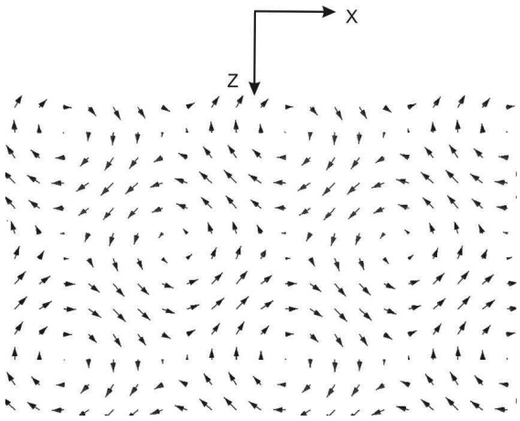

Fig. 6b. 2D distribution of the time-averaged Poynting vectors resulting from the superposition of four waves shown in Figure 6a.

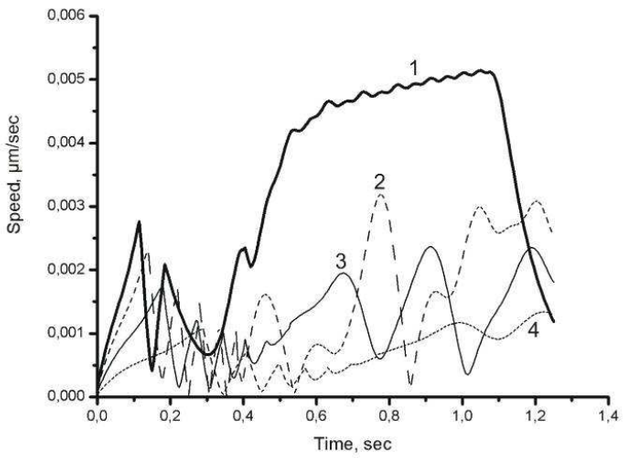

Fig. 7. The variation of motion velocity of a test particles in an averaged field of distributed Poynting vectors with the change of the degree of mutual coherence of the waves (four superposing waves are in phase): curve 1 – one of the waves is incoherent; curves 2, 3, 4 correspond to the degree of coherence 0.25, 0.5, and 0.75, respectively.

Increasing the degree of mutual coherence of the waves sets a more uniform velocity magnitude of moving particles. The magnitude of the resultant force causing this motion under increasing the degree of coherence, practically, does not change with time, see Fig. 8. The maximum depth of modulation for coherent equiphase waves determines the stable position of particles. *The chaotic state and the average particle velocity value can be taken as a possible guideline in estimating the degree of coherence of superposing waves.*

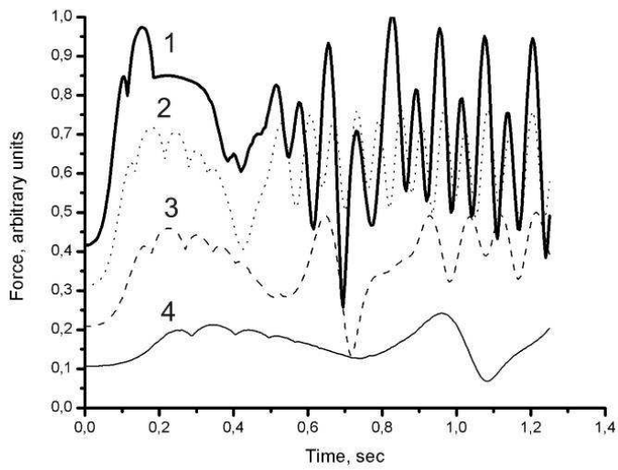

Fig. 8. The change of the resultant force of the test particle motion in the time-averaged field of distributed Poynting vectors with the change of the degree of mutual coherence of the waves (four superposing waves are in phase): curve 1 – one of the waves is incoherent with all other waves; curves 2, 3 and 4 correspond to the degree of coherence of the waves 0.25, 0.5, and 0.75, respectively.

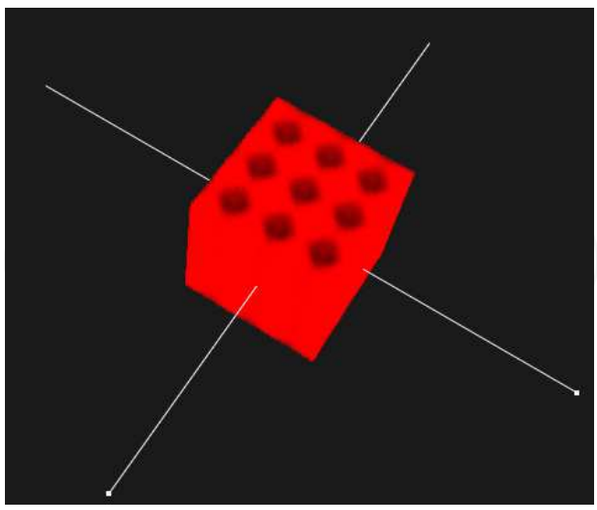

Fig. 9. "Cellular" distribution of the potential traps for microparticles in the case of superposition of four waves.

It is worth emphasizing two issues for the case of superposition of four plane waves. First, the dependence of the depth of modulation for the distribution of the time-averaged

Poynting vectors on the phase relation of superposing waves. It is here assumed that changing the phase relation between the superposed waves causes a transition (in the observed pattern) from the situation when the maxima of two systems of mutually orthogonal standing waves coincide to the case when the nodes of two such systems coincide. Thus, the velocities of particles in such fields depend on the depth of modulation of the distribution of the time-averaged Poynting vector, as it is seen in Fig. 8. Second, the superposition of four waves linearly polarized in the plane of incidence results in forming so-called "cellular" structure in the resulting field distribution, see Fig. 9, which can be used for transfer (transporting) of the set of periodically positioned microparticles *as an entity* to a desired zone.

One considers a future deeper investigation of the peculiarities of motion of microparticles to reveal the coherent characteristics of the waves constituting certain spatial polarization distributions.

The use of strongly reflected test spherical particles provides obtaining more realistic notion on movement of particles in the field modulated in polarization in the incidence plane. So, the test particles are concentrated in zones (planes) of minima of the time-averaged Poynting vector and move along these planes. This situation reflects in the most adequate manner the processes of particle moving in the fields spatially modulated in polarization.

3.3 Experimental technique and results

Direct experimental verification of the results of computer simulation is rather difficult. Spatial period of the polarization distribution resulting from superposition of plane waves meeting at right angle is less than a wavelength of the laser radiation of the visible range. In this case, diagnostics of optical currents presumes the using test particles (preferably spherical) of size much less than the period of polarization distribution. That is why, direct visualization and diagnostics of such particle currents is hampered.

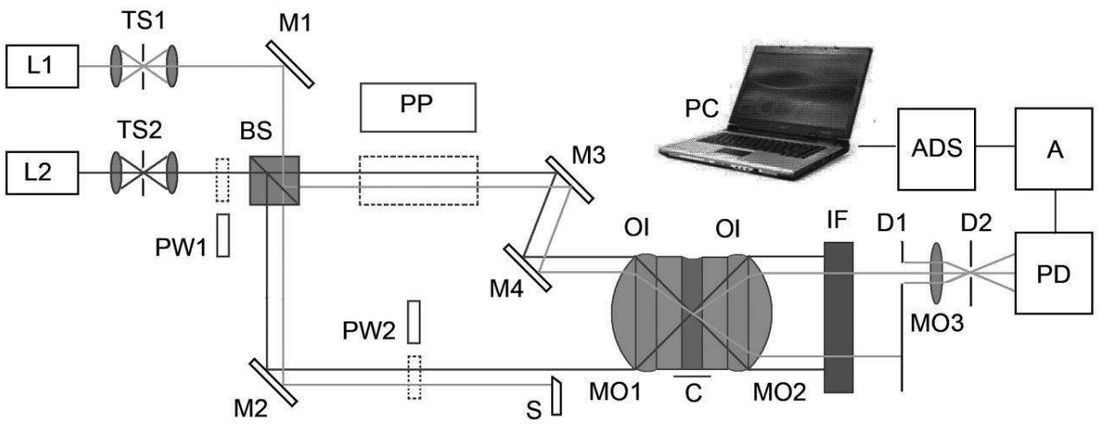

Fig. 10. Experimental setup: L1, L2 - lasers; TS1, TS2 - telescopic systems; M1, M2, M3, M4 - mirrors; PW1, PW2 - half-wave plates for λ=635 nm; PP - plane-parallel plate; BS - beam-splitter; MO1, MO2, MO3 - microobjectives; C - cuvette with gold hydrosol; IF - interference filter at λ=532 nm; D1(0.7-diam), D2 - diaphragms; S - opaque screen; PD - photodetector; A - amplifier; ADC - analog-to-digit converter; PC - computer.

For verifying the results of above consideration and computer simulation, we have studied experimentally the influence of the field resulting from superposition of two plane waves meeting at right angle with various combinations of their states of polarization on the test particles. Experimental arrangement is shown in Fig. 10. To provide right angle between the beam axes, we use immerse-oil-microobjective 90× with NA 1.25. Two parallel linearly polarized beams converge at the focus of microobjective 1. If the electrical vectors of two beams are parallel, the intensity distribution as a set of interference maxima and minima is formed at the area of superposition of such beams. We used radiation from a semiconductor laser RLTMRL-III-635 (λ=635 nm). For that, the period of an interference pattern is 449 nm. For investigation of the influence of the field distribution with such period on the particles, particle's size must be much less than the mentioned period. We have used spherical particles of hydrosol of gold with diameter 40 nm, approximately. Hydrosol have been obtained following the standard technique [53], by mixing of chloroauric acid ($H[AuCl_4]$) and sodium citrate (Na_3Cyt). Let us describe the experimental conditions in more details. Weight concentration of gold particles in water was $5 \cdot 10^{-6} kg/m^3$. Experiment was carried out at room temperature, humidity 65% and air pressure 741 mm Hg. Note, our observation show that modest changing of the experimental conditions against ones mentioned here do not influence appreciably the results of experiment. As a matter of fact, we perform experiment with low-power of laser radiation (not exceeding 5 mW). In this case, one can neglect acoustic waves arising due to thermal action of laser radiation, which would become very important when one operates with high-power impulse laser beams. On these reasons, special precautions, such as use of anechoic chamber, are not undertaken in our study.

Periodical intensity distribution causes movement of the particles and formation of the periodical distribution of concentration of particles as the planes coinciding with interference minima of the intensity distribution at the area of superposition of two beams. These planes can be regarded as the analog of crystallographic planes in crystals. Direct visualization of particles and their currents is hampered due to small particle size. However, at planes of dense packing of particles self-diffraction takes place. We have observed this phenomenon for angles of meeting of two beams less than 40°. For right angle of meeting of the beams, the each self-diffracted beam propagates *along of* and *contrary to* the propagation direction of other of two superposing beams. Thus, it is impossible to discriminate the initial and self-diffracted beams. That is why, taking into account the Bragg law, we use, for diagnostics of periodical distributions of particles, the test laser beam with another wavelength, λ=532 nm. To form the same interference distribution (with the period 449 nm) with such wavelength the angle of meeting of two beams could be 72.6°. So, the angle of incidence of the probing beam must be 36.3° in respect to bisector of the writing beams. In this case, the Bragg law is fulfilled strictly for the probing beam. The mentioned angles are the angles of propagation in light-scattering media, in our case in water.

Two some shifted beams from a green laser (marked by thin line in Fig. 10) propagate in parallel to the beams of red laser (marked by thick line). The external green beam is stopped by the screen S, while the inner probing beam passes the microobjective MO1 and falls at the angle 36.3° into the area of interference extrema. Diameters of the focused beams of red and green lasers are approximately 12 μm and 10 μm, respectively. Glass cuvette C with gold hydrosol is placed at the area of interference pattern. Thickness of the cuvette walls 0.15 mm, and thickness of the swept volume is 18 μm. Oil immersion with refraction index 1.515 is placed between microobjectives MO1 and MO2. Microobjective MO2 is used for adjusting the optical arrangement and output the radiation diffracted on periodical distribution of gold particles.

Optical lengths of two legs of an interferometer BS-M2-M3-M4-MO2 are strictly identical. So, two beams from red laser are mutually coherent and interfere at the focus of the microobjective MO2. Placing a perfect plane-parallel plate PP of thickness 19 mm into one interferometer leg leads to disappearance of interference, while the corresponding optical path difference exceeds the coherence length of red laser. What is important, introducing the plate PP must no be accompanied with shifting beams into interferometer. In such a manner, one can control appearance and disappearance of interference extrema at the focus of MO1.

The change of the position of the plate leads to the change of the photodetector signal. Thus, in the case of superposition of radiations from lasers L1 and L2 which are linearly polarized at the plane perpendicular to the figure plane removal of the plate PP results in increasing signal from a photodetector. It shows forming periodical spatial distribution of gold particles and appearance of the diffracted probing beam. The diffracted signal appears for radiation power of red laser more than 2 mW. However, it has been observed that for radiation power exceeding 50 mW, non-linear effects occur in light-scattering medium. So, gold particles absorb radiation and heat environment, acting as a thermal lens. That is why we have carried out our experiment for radiation power of red laser 5 mW. Radiation power of the probing beam was 0.5 mW, so that it can not affect gold particles.

If two beams of red laser are polarized in the figure plane (half-wavelength plate PW1 for λ=635 nm is inserted) and their convergence angle is equal to 90°, only polarization modulation takes place in the incidence plane. In this case the diffracted probing beam is present as well. The signal at the photodetector output with and without plane-parallel plate is shown in Fig. 11 b. The diffracted probing beam is present, but is approximately of half the intensity in comparison with the case illustrated in Fig. 11 a. This experimental result is also in accordance with the result of computer simulation. The spatially modulated in polarization field (in the plane of incidence) is correlated with concentration of the test particles at the planes of minima of the time-averaged magnitude of the Poynting vector, and particles move along these planes.

If two beams form red laser are linearly polarized, but one of them in the figure plane while another one perpendicularly to this plane (a half-wave plate PW2 for λ=635 nm is inserted), the diffracted probing beam is absent, cf. Fig. 11 c. This shows that at the focal plane where the beams from red laser superpose, the periodical distributions of gold particles are absent. This experimental result is also in agreement with earlier computer simulation [42]. In other words, there are no any ordered optical currents being liable to optical diagnostics, as it has been made in previous case.

Thus, temporal and space peculiarities of particle's motion in optical fields without intensity modulation, but only due to polarization modulation causing the spatial modulation of the time-averaged Poynting vector (depending on the degree of mutual coherence of superpose waves) opens up new feasibilities for the use of such field characteristics and the parameters of microparticles motion for estimating the temporal coherence of the tested field. Here we have demonstrated a possibility of influence of only the polarization factor on formation of optical currents in liquids by the use of the principles of spatial polarization modulation in the observation plane. Besides, we have shown the possibility of diagnostics of optical currents using test particles of nanoscale.

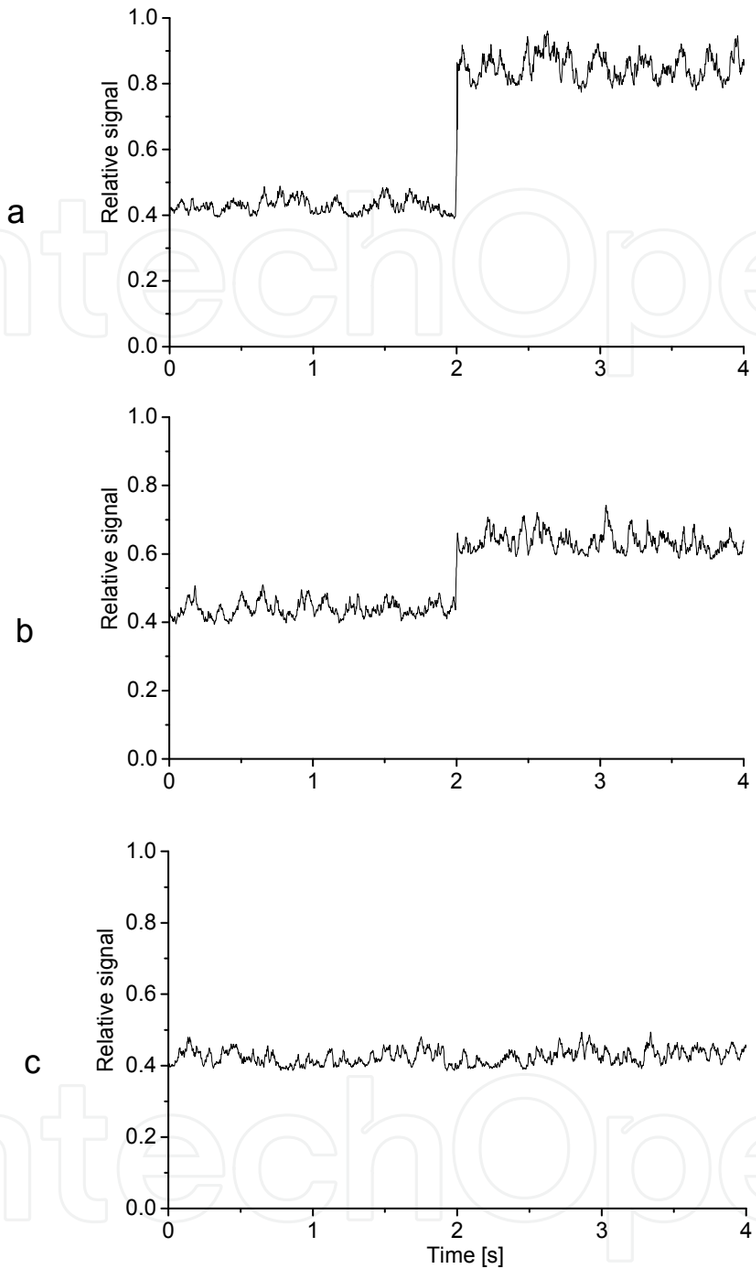

Fig. 11. Relative signal of a photodetector (a plate PP is inserted on 2 sec and then removed) in the case when radiation of red laser is linearly polarized: (a) both beams are polarized in the plane perpendicular to the figure plane; (b) both beams are polarized in the figure plane; (c) one beam is polarized at the figure plane, while another one is polarized perpendicularly to this plane.

The explained metrology of microstructure of optical fields may be extended, to all appearance, on polychromatic waves. The initial steps in this direction have been recently made in studies [52, 54 – 60].

4. Polarization singularities in partially coherent light beams

In this section we describe specific polarization singularities arising in incoherent superposition of coaxial orthogonally polarized laser beams. It is shown that in transversal cross-section of paraxial combined optical beams of this class, instead of common singularities, such as amplitude zeroes (optical vortices) inherent in scalar fields [2], and polarization singularities such as C points and L lines inherent in completely coherent vector fields [18], *phase singularities of the complex degree of polarization* (CDP) arise, whose description and investigation have been initiated by papers [61 - 65] basing on earlier studies [66 - 68] concerned to the Young's concept of the edge diffraction wave in connection with diagnostics of phase singularities of spatial correlation functions of optical fields. There are U contours along which the degree of polarization equals zero and the state of polarization is undetermined (singular), and isolated P points where the degree of polarization equals unity and the state of polarization is determined by the non-vanishing component of the combined beam. (Note, discussed here notion of CDP differs from the definition of the complex degree of mutual polarization, CDMP [6] that is two-point function of an optical beam.)

Let us briefly argue the relevance of the introduced approach.

It is known [69] that each level of description of optical phenomena possesses its own set of singularities, *i.e.* the set of elements of a field (points, lines, surfaces, depending on considered dimension) where some parameter of a field is undetermined. Importance of detecting such elements of a field is caused by the fact that such elements form peculiar skeleton of a field, so that if one knows behavior of a field at such singular elements (and at nearest vicinities of them), one just can predict, at least in qualitative manner, but with high level of validity, behavior of a field at all other areas.

Conditionally, one can classify singularities of optical fields in the following manner [69]:

- singularities of geometrical optics,
- singularities of completely coherent scalar (homogeneously polarized) wave fields – optical vortices,
- singularities of completely coherent vector (inhomogeneously polarized) wave fields – optical vortices,
- singularities of partially coherent wave fields,
- singularities of quantum optics – "quantum cores".

Singularities of geometrical optics are caustics where the field amplitude reaches infinity. Singularities of completely coherent wave fields are divided into two sub-classes: (i) for scalar (homogeneously polarized) fields and (ii) for vector (inhomogeneously polarized) fields. In scalar fields, when polarization can be neglected, so-called wave front dislocations take place (which are also referred to as amplitude zeroes or optical vortices). Phase of the complex amplitude is undetermined at such elements and is step-like changed at crossing of them. In vector fields optical vortices are absent, though they remain in any polarization ("scalar") component. Instead of vortices, polarization singularities arise at cross-section of a field, *viz.* field elements where azimuth of polarization (C points) or handedness (L lines) is

undetermined [18]. Vector skeletons of coherent inhomogeneously polarized fields were elaborated in details in papers [70 - 72]. By crossing L lines, handedness is step-like changed into opposite one; by crossing C point, azimuth of polarization is changed into orthogonal one. These types of singularities are blurred in quantum-mechanical description being "camouflaged" by so-called quantum vacuum [69], though the distance of influence of such quantum core is rather small. Its linear size is of order of magnitude λ^{-3} (about 6 Å for He-Ne laser).

All mentioned singularities disappear in the case of partially coherent wave fields (though they remain in each completely coherent component, mode in a set of which partially coherent radiation is decomposed. Instead (beside) of them, new singularities appear inherent just in partially coherent fields. Let us emphasize, that singularities of partially coherent fields have formed the novel topic in the field of singular optics just at the beginning of the Third Millenium [3].

For that, two situations arise again: (i) scalar case when polarization can be ignored while the state of polarization is the same at all point of a field, and (ii) vector case when the state of polarization of *partially coherent* field changes from point to point that requires explicit taking into account of vector nature of light. The first (scalar) case became the subject of intense investigations in last years [67, 73 - 76]. As a result of these investigations, new phase singularities of spatial and temporal correlation functions of quasi-monochromatic light fields have been revealed, as well as singularities of spectral components of polychromatic ("white-light") radiation [68, 77 - 82]. For that, vector singularities of partially coherent light fields have been revealed just recently [61 - 65]. Such singularities are elaborated in this section.

4.1 U and P singularities in partially spatially coherent combined beams

Let us consider vector singularities in partially coherent optical beams by giving the following simple instructive example. Mutually incoherent and orthogonally polarized Laguerre-Gaussian mode LG01 and a plane wave are coaxially mixed. Such components can be obtained from one laser (using a computer-generated hologram for forming LG01 mode) in interferometric arrangement with optical delay, Δl, considerably exceeding a coherence length of the used laser, l, or using two different lasers. Intensity of a plane wave is set deliberately to be less than the peak intensity of the mode, see Fig. 12.

Thus, we consider two-component mixture co-directional orthogonally polarized beams, one of which contains a common phase singularity, *viz.* optical vortex. Interference between such beams with forming common interference fringes is excluded by two reasons: (i) specified mutual incoherence of the components: (ii) polarization orthogonality of them. Note, even only the second condition *per si* determines that, independently on the degree of mutual coherence of two beams over whole interval from zero (for optical path difference exceeding the coherence length) to unity (for zero optical path difference) *visually* observed and *photometrically* measured pattern remains unchangeable. However, more delicate polarization analysis of the combined beam enables to differentiate two limiting cases, *viz.* completely coherent and completely incoherent mixing of orthogonally polarized components.

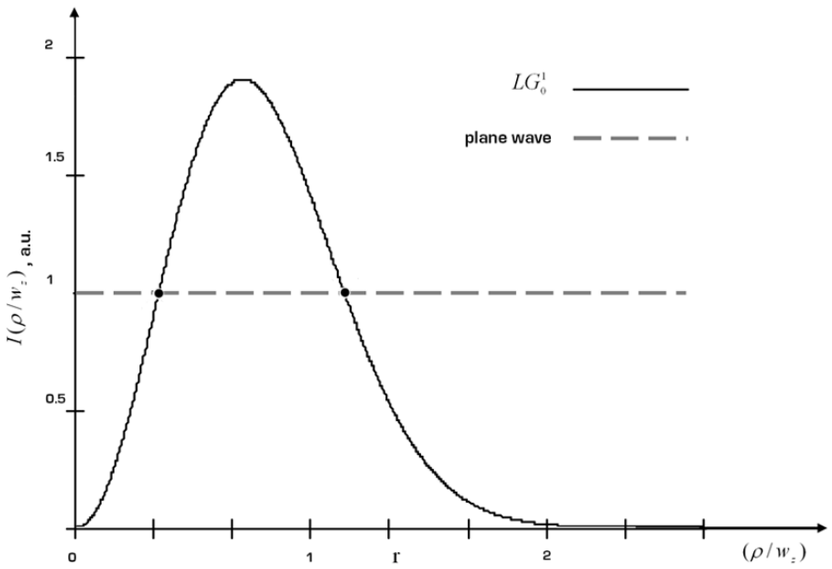

Fig. 12. Mixing of vortex-supporting LG01 mode and plane wave with intensity less than peak intensity of a mode.

Let us firstly consider the limiting case when two components are completely mutually coherent. For the sake of distinctness (and for substantiveness of further consideration), we consider coherent mixing of orthogonally *circularly* polarized LG01 mode and a plane wave. Beside of all, choice of circular polarization basis possesses the advantage that it is invariant in respect to rotation of the coordinates, in contrast to linear or elliptical basis, which are relative ones [83].

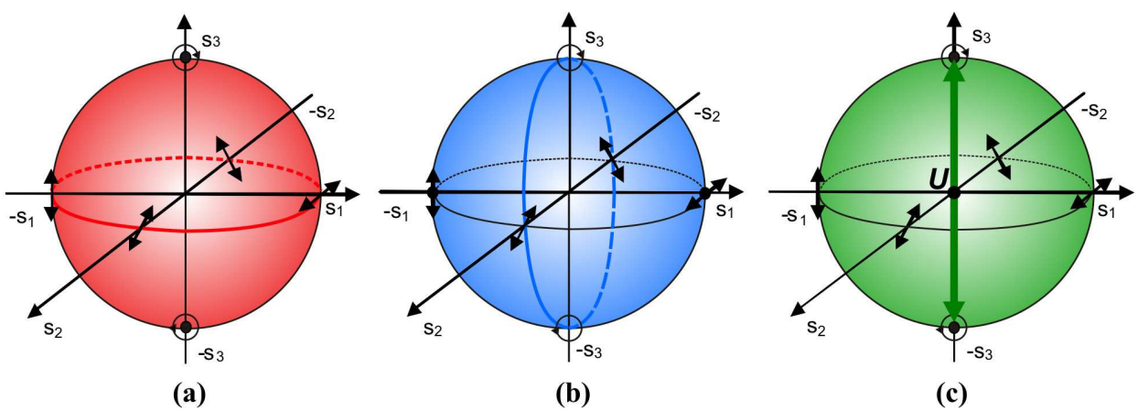

Fig. 13. The lines of equal intensities of orthogonally polarized beams at Stokes space: equator of the Poincare sphere for circular polarization basis, coherent mixing (a); 45°-meridian including the poles for linear polarization basis, coherent mixing (b); diameter of the Poincare sphere connecting the poles for circular polarization basis, incoherent mixing (c).

In general, combined beam, everywhere with the unit polarization degree ($\sqrt{s_1^2 + s_2^2 + s_3^2} = 1$, where s_1, s_2, s_3 are the normalized second, third and fourth Stokes parameters, respectively [17, 83, 84], is elliptically polarized. But at the center of vortex of LG01 mode the field is circularly polarized with the state of polarization of a plane wave. A common phase singularity (vortex) of orthogonally polarized component of the combined beam lies at the bottom of this circular polarization. At the same time, the resulting field is polarized linearly at two contours where amplitudes of two components become equal to each other, see Fig. 13 a.

For that, owing to helicoidal structure of a wave front of LG01 mode, azimuth of linear polarization changes with changing phase difference of a mode and a plane wave. Such topological structure can be considered as elementary experimental model of the assemblage of C point and surrounding it L contour of conventional singular optics of vector fields. Really, similarly to the case of random vector fields, crossing L line where handedness is undetermined is accompanied by step-like changing handedness into opposite one, corresponding to predominant in intensity component with unchangeable azimuth of polarization. For comparison, Fig. 13 b illustrates the line of equal intensities of coherently mixed components in linear polarization basis.

It is of interest that the elementary structure shown in Fig. 13 a is directly related with description of polarized light at the circular complex polarization plane that is a stereographic projection of the Poincare sphere [84]. So, C point and L contours correspond to the pole of the Poincare sphere and its equator, see Fig. 14.

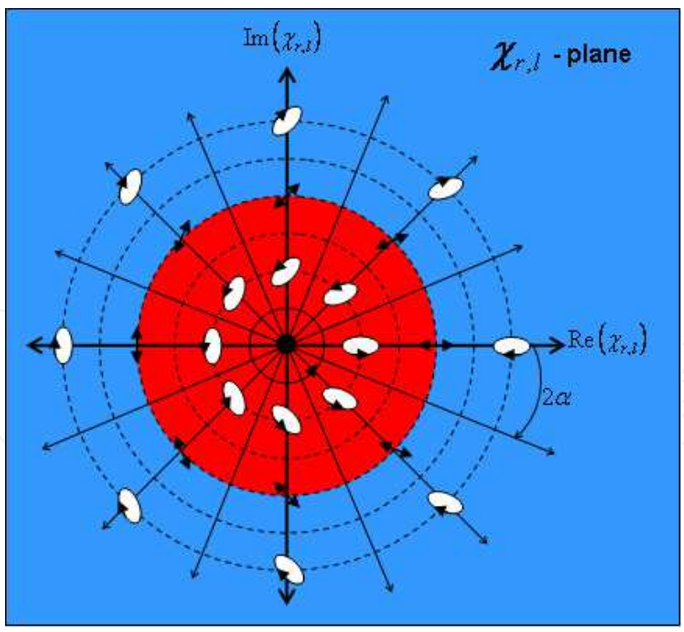

Fig. 14. The complex circular polarization plane. The center of coordinates corresponds to left-circular polarization (C point); the circle of unite radius separating red and blue areas corresponds to linear polarizations with changeable azimuth of polarization (L contours), its contours separate the area of the beam with left handedness (red) and right handedness (blue); right-circular polarization point lies at infinity.

Let us support this intuitive consideration by formal description. Let us proceed from Jones vectors of two components, right-circularly polarized LG01 mode and left-circularly polarized plane wave,

$$\mathbf{E}_{LG} = c\left(w/\rho\right)\exp\left(i\Delta\right)\begin{bmatrix}\exp\left(i\varphi\right)\\ \exp\left[i\left(\varphi+\pi/2\right)\right]\end{bmatrix},\ \mathbf{E}_{P} = \begin{bmatrix}\exp\left(i\varphi\right)\\ \exp\left[i\left(\varphi-\pi/2\right)\right]\end{bmatrix}, \tag{5}$$

where c is the amplitude factor corresponding to inhomogeneous amplitude distribution of a mode as a function of dimensionless radial coordinate, and $e^{i\Delta}$ is associated with helicoidal change of a phase of a mode under circumference of the central vortex (its explicit form for Laguerre-Gaussian mode is well known but is not relevant here). There is Jones vector of the combined beam:

$$\mathbf{E}_{Total} = \mathbf{E}_{LG} + \mathbf{E}_{P} = \begin{bmatrix}E_x\\ E_y\end{bmatrix} = \begin{bmatrix}c\exp\left(i\Delta\right)+1\\ c\exp\left[i\left(\Delta+\pi/2\right)\right]+\exp\left(-i\,\pi/2\right)\end{bmatrix}\exp\left(i\varphi\right) \tag{6}$$

General coherency matrix of the beam is found as

$$\left\{\mathbf{J}\right\} = \mathbf{E}_{Total}\cdot\mathbf{E}^{*}_{Total} = \begin{bmatrix}E_x\\ E_y\end{bmatrix}\begin{bmatrix}E^{*}_x & E^{*}_y\end{bmatrix} = \begin{Vmatrix}J_{xx} & J_{xy}\\ J_{yx} & J_{yy}\end{Vmatrix}, \tag{7}$$

or in explicit form:

$$\left\{\mathbf{J}\right\} = \begin{Vmatrix}c^2+2c\cos\Delta+1 & c^2\exp\left(-i\,\pi/2\right)+2c\sin\Delta+\exp\left(i\,\pi/2\right)\\ c^2\exp\left(i\,\pi/2\right)+2\sin\Delta+\exp\left(-i\,\pi/2\right) & c^2-2c\cos\Delta+1\end{Vmatrix} \tag{8}$$

Combining the elements of coherency matrix, one can find *full* Stokes parameters:

$$\begin{gathered}S_0 = J_{xx}+J_{yy} = 2(c^2+1);\qquad S_1 = J_{xx}-J_{yy} = 4c\cos\Delta;\\ S_2 = J_{xy}+J_{yx} = 4c\sin\Delta;\qquad S_3 = i\left(J_{xy}-J_{yx}\right) = 2(c^2-1).\end{gathered} \tag{9}$$

Here we are especially interested in the case when $c=1$. One just obtains for this case the *normalized* Stokes parameters:

$$s_0 = 1;\quad s_1 = \cos\Delta;\quad s_2 = \sin\Delta;\quad s_3 = 0. \tag{10}$$

Vanishing of the fourth Stokes parameter means that polarization at all points of the contour where intensities of the mixed components are equal to each other are equally distanced from the states of polarization of the components, i.e. neither right-circular nor left-circular predominate in intensity. It is in direct correspondence with Fig. 13 a. At all points of such L contour polarization is linear with the polarization azimuth $\alpha = 0.5\tan^{-1}\left(s_2/s_1\right) = \Delta/2$, while the angle of ellipticity $\beta = 0.5\arcsin s_3 = 0$. Besides, the degree of polarization $P = \sqrt{s_1^2+s_2^2} \equiv 1$. In correspondence with helicoidal structure of a wave front of LG01 mode,

a phase difference of the components changes along the contour of equal intensities that results in changing azimuth of polarization. Thus, we obtain direct analog of L contour. Further, at the center of vortex of LG01 mode we have $c = 0$. Again, proceeding from Eq. (9) we find the normalized Stokes parameters $1,\ 0,\ 0,\ -1$, i.e. left-circular polarization of a plane wave. In the vicinity of such C point polarization is elliptical, with the azimuth of polarization changing with azimuthal coordinate and ellipticity decreasing from the vortex to L contour, Eq. (10), where handedness is undetermined an step-like changing by crossing this contour. It is all in quite correspondence with Fig. 14.

Thus, for circular polarization basis walking along contour of the combined beam "LG01 mode + plane wave" where intensities of the components become equal corresponds to moving along equator of the Poincare sphere that is determined only by the ratio of the second and third Stokes parameters. (For comparison, using linear polarization basis, to say 0° and 90°, one obtains by the same way the normalized Stokes parameters for the combined beam $1,\ 0,\ \cos\left[\Delta + (\varphi_0 - \varphi_{90})\right],\ \sin\left[\Delta + (\varphi_0 - \varphi_{90})\right]$ that corresponds to points of 45°-merdian of the Poincare sphere, see Fig. 13 b.)

Before consideration of the most general case of partial mutual coherence of the mixed orthogonally polarized components in the following section, let us consider other limiting case, *viz.* completely incoherent mixing of such components. There is no necessity to proceed now from Jones vectors and to form a coherency matrix of the combined beam. One can at once determine the Stokes parameters of mutually incoherent components and to sum directly them, without accounting phase relations that are irrelevant for incoherent summation. The normalized Stokes parameters of orthogonally polarized beams differ only in sign of the second, third and fourth parameters: $\{1,\ s_1,\ s_2,\ s_3\}$ and $\{1,\ -s_1,\ -s_2,\ -s_3\}$. It is clear that when two components become equal in intensities, the normalized Stokes parameters of the combined beam becomes $\{1,\ 0,\ 0,\ 0\}$. The field at such elements of a field is completely unpolarized. There are just U singularities [61 - 63]. This case is shown in Fig. 13 c for the case of incoherent mixing of orthogonally circularly polarizer components. Trajectory of the imaging point for the combined beam in this case is the diameter of the Poincare sphere connecting two poles. U singularity is imaged by the center of this sphere, and all other points (beside the center and poles) image partially circularly polarized fields. For that, the length of a vector drawn from the center of the Poincare sphere to the imaging point inside it equals the degree of polarization. The point where the degree of polarization equals unity is referred to as P (completely polarized) point [61 - 63]. Its location is determined by the vortex of orthogonally polarized (scalar singular) component. The set of P points and U contours corresponding to extrema of the degree of polarization of a field are *the singularities of the degree of polarization* forming the vector skeleton of two-component mixture of orthogonally polarized beams. Note, in papers [61 - 64] consideration is carried out using the notion of the complex degree of polarization – CDP, associated with orientation of the vector of polarization in the Stokes space and undergoing the phase singularity at the center of this space. So, U singularities can be considered just as vector singularities, *viz.* singularities of the vector of polarization, when its magnitude equals zero and a phase (orientation of the vector) is undetermined.

Let us emphasize that the condition of occurring U singularity is equal to the condition of occurring L contour in completely coherent limit. It means that loci of C and L singularities in completely coherent fields and P and U singularities in partially coherent fields arising from completely incoherent orthogonally polarized components, correspondingly, coincide.

Displacement from U singularity results in predomination of one of two orthogonal components in intensity. The state of (partial) polarization is just determined by the predominant component. That is why, the degree of polarization can be determined in similar form as visibility:

$$P = \left| \frac{I_1 - I_2}{I_1 + I_2} \right|. \tag{11}$$

In other words, at each point of the combined beam equal in intensities parts of orthogonal components form unpolarized background, at which manifests itself completely polarized part corresponding to predominant in intensity component. This is in a complete agreement with classical decomposition of partially polarized beam into completely coherent and completely incoherent parts, which are added on intensities, without accounting phase relations [17, 84]. Note, there are no any device providing such decomposition in practice. However, share of completely polarized part can be determined experimentally through the Stokes polarimetric experiment, $P = \sqrt{s_1^2 + s_2^2 + s_3^2}$ or, equivalently, following Eq. (11). In theory one put in correspondence to such beams the set of two coherency matrices – for completely polarized and completely unpolarized parts of a beam [1, 17].

Thus, only two orthogonal states of polarization take place in combined beams of considered kind, which are separated by U singularities where the state of polarization is undetermined.

So, the considered limiting cases show the same location of C and P singularities and L and U singularities for the same set of components. However, vicinities of such singularities are essentially different. Only two orthogonal states of polarization are present in spatially partially coherent combined beams, and only the degree of polarization changes from point to point within the areas separated by U singularities.

4.2 Vector singularities for partially mutually coherent mixed components

Let us consider now the most general case, when two mixed components shown in Fig. 12 are orthogonally (circularly) polarized and are partially mutually coherent, so that the degree of mutual coherence of the components can be gradually changed from unity to zero. It can be implemented in the arrangement of the Mach-Zehnder interferometer with controllable optical pass difference between the legs of an interferometer, as shown in Fig. 15.

A half-wave plate at the interferometer input serves for fine balancing of intensity ratio between the legs of an interferometer without changing total intensity at its output. Two polarizers inside an interferometer are controllers setting orthogonal linear polarizations. LG01 mode is generated by a computer synthesized hologram. A quarter-wave plate at the output of an interferometer transforms orthogonal linear polarization into orthogonal circular ones.

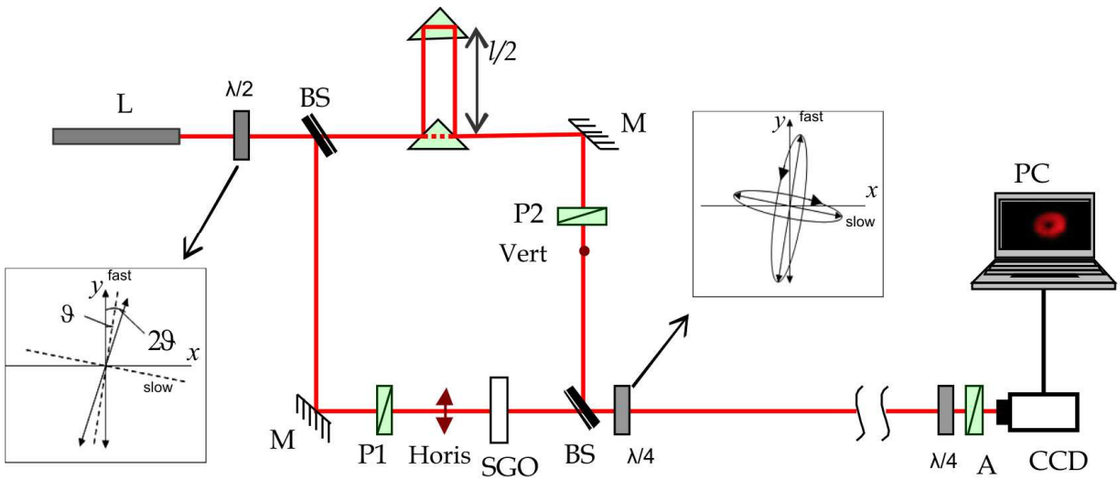

Fig. 15. General arrangement for generation and detection of vector singularities in partially coherent beams: L – He-Ne laser; $\lambda/2$ and $\lambda/4$ – half-wave and quarter-wave plates, respectively; P – polarizers; A – linear analyzer; SGO – singularity generating object (computer synthesized hologram); BS – beam splitters; M – mirrors; CCD – CCD-camera; PC – personal computer. Insets show action $\lambda/2$ and $\lambda/4$ plates at the input and at the output of an interferometer; two prisms form optical path delay loop.

A quarter-wave plate and linear analyzer at the receiving end, together with CCD-camera matched with personal computer serve for Stokes-polarimetric analysis of combined beams. Two prisms at one of legs of an interferometer enable to control optical path difference and mutual coherence of the mixed components. Namely, one can control path delay Δl from zero to magnitude exceeding a coherence length (length of wave train) l of the used laser. Change of the ratio $\Delta l/l$ corresponds to change degree of mutual coherence of orthogonally polarized components. Thus, for $0 < \Delta l/l < 1$ the combined beam is *simultaneously* partially spatially coherent (due to changing intensity ratio at cross-section of the resulting field) and partially temporally coherent (due to non-zero optical path difference between the components), one expects for increasing optical path difference the following.

As it has been mentioned above, the condition of arising of L contours and U contours in the limiting cases of mixing of orthogonally circularly polarized beams is the same: intensities of the components must be equal to each other. If the optical path difference increases from zero, field at the L contour remains linearly polarized, but the degree of polarization decreases. It follows from that the degree of polarization of a beam is determined by the degree of mutual coherence of its arbitrary orthogonal components [1, 17], here right-hand and left-hand circular components. It means that *U contour nucleates just at the bottom of L contour.*

The degree of polarization can be represented equivalently in terms of *measured* Stokes parameters (that will be used in the next section) or *theoretically*, *viz.* through the invariants

of the coherency matrix, which at the same time determine coherence properties of a field [17]:

$$P = \sqrt{1 - \frac{4\det\{\mathbf{J}\}}{\mathrm{Sp}^2\{\mathbf{J}\}}}\,. \tag{12}$$

For that, in general, the degree of polarization is always non less than modulo of the degree of mutual coherence of the components, for circularly polarized components

$$\left|\mu_{rl}\right| = \left|\frac{J_{rl}}{\sqrt{J_{rr}J_{ll}}}\right|. \tag{13}$$

In general case, $P \neq \left|\mu_{rl}\right|$, as the degree of coherence depends on the decomposition basis while the degree of polarization is invariant [5]. However, it has been shown [1, 17] that the degree of polarization is equal to the *maximal* degree of coherence, $P \equiv \left|\mu_{rl}\right|_{\max}$, in the case when the components are of equal intensities. This is just the case of L singularities and U singularities. It is of the most importance, that change of the optical path difference changes weights $\left|\mu_{rl}\right|$ of completely coherent (and completely polarized) part of the combined beam and $1-\left|\mu_{rl}\right|$ of its completely incoherent part. Increasing $\Delta l/l$ difference corresponds to increasing of weight of U singularity against L singularity, so that one can follow gradual transformation of L contour into U contour.

4.3 Experimental reconstruction of "pure" and "mixed" polarization singularities

Mixing of LG01 mode and plane wave was performed in the arrangement Fig. 15 [66]. Intensity of a plane wave was considerably (approximately by the order of magnitude) less the peak intensity of a mode, both circularly (orthogonally) polarized. The following results have been obtained under such conditions.

Fig. 16 shows the combined beam whose view, as was mentioned above, within experimental accuracy remains the same at arbitrary optical path delay set in the interferometer. This photo has been obtained for incoherent mixing of two components for $\Delta l/l \approx 3$ (under condition realized in paper [68]. We measured spatial distribution of the Stokes parameters and looked for the elements where $s_1 = s_2 = s_3 = 0$ ($P = 0$, U contours), and $s_3 = 1$ (P point), see discussion after Eq. (10). In such a manner, we were in a position to reconstruct a vector skeleton of partially spatially coherent combined beam formed by completely mutually incoherent components, as in Refs [61 - 64]. Experimental error in determining the normalized Stokes parameters was at the level 7%; this determines reliability with which we reconstructed P point and U contours. P and U singularities for this case are shown in right fragment of Fig. 16. Two U contours separate the areas with right-circular and left-circular polarization shown by different colors. Within these areas $\sqrt{s_1^2 + s_2^2} = 0$, while $s_3 < 1$. Let us emphasize that the full Stokes-polarimetric experiment over combined beam cross-section is necessary in this case, as operating only with rotating linear analyzer does not provide differentiation partial circular polarization from complete elliptical polarization.

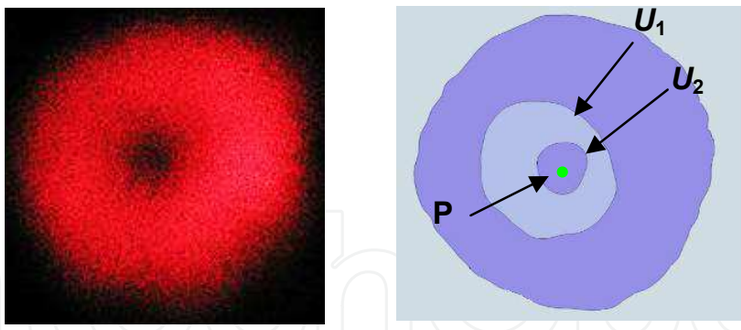

Fig. 16. The partially coherent combined beam (left) and its vector skeleton formed by P and U singularities (right) for completely incoherent mixing of circularly polarized components.

Separate maps of the Stokes parameters are less representative being only row material for finding out the degree of polarization, ellipsometric parameters of a field, and vector singularities. That is why, we demonstrate separately from 2D pattern shown in right fragment of Fig. 16 1D cross-section of the degree of polarization of this combined beam, see Fig. 17. Red curve shows two-lateral radial dependence of P computed following Eq. (11). Blue curve shows experimentally obtained distribution found as the combination of measured Stokes parameters, here $P = |s_3|$. Quantitative discrepancy of two curves (both in positions of zeroes and in heights of side-lobes) is obvious and is explained by anisotropy of the vortex. Nevertheless, behavior of the experimental dependence is in quite satisfactory qualitative agreement with the simulation results. Namely, one observes two zeroes of the degree of polarization at the each side of the central optical vortex that are the signs of two U contours. Moreover, experiment has proved typical conical vicinity of U contours recently predicted and observed in paper [61], which are reliable sign of true singularity of any kind, in contrast to local minimum.

Another limiting case (completely mutually coherent components) for $\Delta l / l << 1$ (approximately 0.05) is illustrated in Fig. 18. Again, spatial maps of the Stokes parameters were obtained and the elements $s_3 = 0$ and $\sqrt{s_1^2 + s_2^2} = 1$ where selected. There are the lines of linear polarization. Than, in several selected points of such L lines we determined the azimuth of polarization, again, by two ways: firstly as $\tan^{-1}(s_2 / s_1)$, and, secondary, as direct measurement of the azimuth of polarization by rotating a linear analyzed up to complete extinction of a field at the specified point that corresponds to crossed azimuth of polarization of the combined beam and the axis of maximal transmittance of analyzer. Description between two results for determining of the azimuth of polarization do not exceeded 0.1 rad.

Perfect extinction of a beam at the specified points just shows that the degree of polarization $P = 1$ (in contrast to the previous case of completely mutually incoherent components, where intensity at the analyzer output is independent on its orientation). Also, for certain orientations of a quarter-wave plate and analyzer, the field at each other point can be extinguished that shows that everywhere the degree of (elliptical) polarization equals unity. It is worth to compare Fig. 18 with a view of the circular complex polarization plane (Fig. 14) to be convincing of that, really, such polarization distribution over of a combined beam is close experimental analogue of the circular polarization plane.

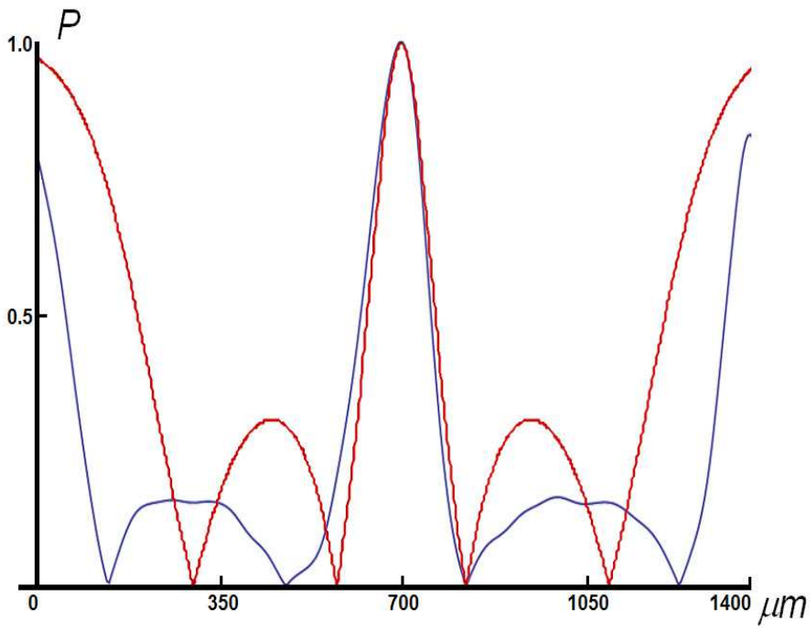

Fig. 17. 1D distribution of the degree of polarization of the combined beam formed by two mutually incoherent orthogonally polarized components defined in Fig.12 and shown in Fig. 16.

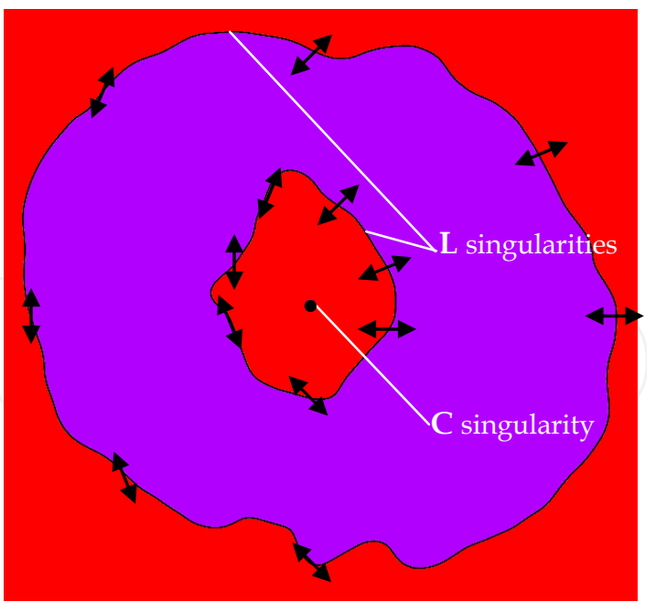

Fig. 18. C and L singularities in combined beam assembled from completely mutual coherent orthogonally (circularly) polarized LG01 mode and plane wave. At L lines, where intensities of two mixed component are equal, the azimuth of polarization changes in agreement of prediction illustrated in Fig. 14 Areas of different colors correspond to opposite handedness.

At last, we have elaborated experimentally intermediate case, when $0 < \Delta l/l < 1$, lying between ones considered above. For step-by-step increasing optical path difference between the same orthogonally (circularly) polarized components, we obtained spatial distributions for the Stokes components I_0, I_{90}, I_{+45}, I_{-45}, I_r, I_l and found from them the Stokes parameters. Further, the degree of polarization and ellipsometric parameters of the combined beam were determined as the combinations of these parameters.

Before formulating the conclusions from our observations, let us represent one of row (intermediate) results undergoing following processing. Fig. 19 illustrates combined beams "LG01 mode + plane wave" (with large intensity ratio, so that one does not visualizes a plane wave) for relative optical path differences close to unity (coherent limit illustrated in Fig. 18) and slightly exceeding a half of the coherence length of used laser, left fragments of Fig. 19. Other fragments of this figure are the intensity distributions I_{+45} (central column) and I_{-45} (right column) used for forming the third Stokes parameters. (Other pairs of intensity distributions show the same tendency). Though two orthogonally polarized components do not interfere, their equal polarization projections selected by properly oriented polarizer *can* interfere depending on their mutual coherence. If the degree of mutual coherence of the components is not zero, their equally polarized projections interfere with forming typical patterns indicating phase singularity. To have enough spatial resolution for determining place of vortex, we set non-zero interference angle between the components (which as small enough to be no influencing on accuracy of polarization measurements). For that, instead of snail-like pattern typical for coaxial mixing of LG01 mode and a plane wave, we obtained interference forklets. Comparison of the central and left columns of Fig. 19 shows that spatial intensity distributions for orthogonal polarization projection of the combined beam are complementary in a sense that dark forklet is replaced by bright one.

The main conclusion follows from comparison of fragments b and e (c and f). Decreasing of the mutual coherence of the mixed components and decreasing of the degree of polarization of the combined beam are accompanied by decreasing of ability of equal polarization projections of the mixed components to interfere that manifests itself in decreasing of visibility of interference pattern. So, in fragments b and c of Fig. 19 ($\Delta l/l \approx 0.05$) the measured visibility is 0.97, while in the fragments Fig. 19 e and f ($\Delta l/l \approx 0.56$) visibility is 0.24 (with experimental error non exceeding 5%). It shows the feasibility allows determine *the degree of mutual coherence* of two orthogonally polarized beams by measuring *the degree of polarization* of the combined beam formed by such components found from Stokes parameters. Namely, in our experiment $|\mu_{rl}|$ for $\Delta l/l \approx 0.56$ also equals 0.24. For the reasons discussed in Section 3, such measurements are preferably be performed at the elements of the combined beam where intensities of two beams are equal to each other (where L and U singularities co-exist in case of partial mutual coherence of the components), while at such singular elements of the combined beam $P \equiv |\mu_{rl}|$.

Thus, vector singularities occurring in light fields, which are simultaneously partially spatially and partially temporally coherent have been considered. It has been shown that in the case of partially coherent mixing of two orthogonally *circularly* polarized components conventional vector singularities, *viz.* C points and L lines submerged in a field of elliptical

polarizations coexist with singularities arising just in partially coherent fields, such as U and P singularities as the extrema of the degree of polarization. Gradual transformation of C and L singularities into P and U singularities, respectively, accompanying decreasing degree of mutual coherence of the components has been experimentally shown. So, conventional polarization singularities of completely coherent fields (C points and L lines) are vanish in incoherent part of the combined beam, so that the only polarization of the component predominant in intensity remains in the vicinities of P points and U lines.

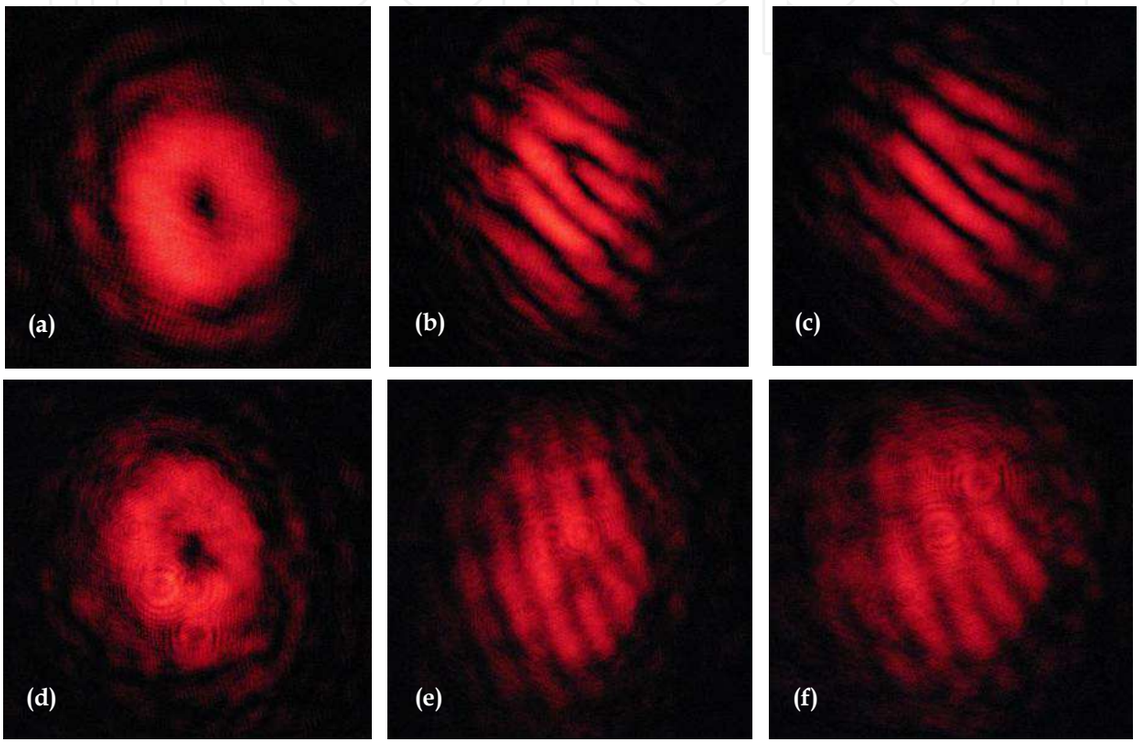

Fig. 19. The combined beams "LG01 mode + plane wave" with relative optical path differences $\Delta l/l \approx 0.05$ (a) and $\Delta l/l \approx 0.56$ (d); the corresponding intensity distributions behind a linear analyzer for determining the third Stokes parameters: +45° (b and e) and –45° (c and f). Decreasing visibility of interference fringes in fragments e and f corresponds to decreasing in parallel the degree of mutual coherence of the mixed components and the degree of polarization of the combined beam.

5. Feasibilities for experimental analysis of characteristics of the Poynting vector components

In this section, potentiality of experimental analysis for the time-averaged Poyntig vector is considered. In part, we will show that combined application of conventional interferometry and Stokes-polarimetry should allow of unambiguous determining characteristics of the time-averaged Poynting vector components at each point of electromagnetic field.

One of theoretical aspects in rapidly developing area of the modern optical technology, elaboration of new kinds of optical tweezers [25 - 30, 85] is connected with the fact that the vortex beams and polarized waves (both homogeneous and inhomogeneous) possess an angular momentum [85 - 87]. Existence of controlled angular momentum provides a possibility for controlled rotation of micro-objects locked by corresponding optical traps. Angular momentum of a field can be specified at each spatial point. One may also consider angular momentum averaged over some spatial area. As it is known [86, 88], angular momentum may be divided into a spin momentum associated with circular polarization, and an orbital one produced by specific beam structure. However, density of the angular momentum, j_z, (at least, of its orbital part) depends upon the location of the axis $\mathbf{r} = 0$ (i.e., "purchase") with regard to which the parameter j_z is calculated. As a result, some ambiguity appears. At the same time, another physical value closely associated with the angular momentum, *viz.* the space distribution of characteristics of the time-averaged Poynting vector (more accurately, its transverse component), represents a univocal function of coordinates of each field point.

Distribution of parameters of the time-averaged Poynting vector for Laguerre-Gaussian beams has been considered in [89, 90]. However, behavior of the time-averaged Poynting vector was analyzed only for homogeneously polarized fields and "symmetrical" beams [86, 89].

At the same time, analyzed fields may be more complicated, in part, when their polarization is inhomogeneous. Distribution of the transverse component of the Poynting vector for such fields may be characterized by a set of certain points, i.e., by the net of Poynting vector singularities [87]. The importance of these points comes from the fact that the characteristics of this singular net, such as the Poynting field skeleton, determine qualitative behavior of the Poynting vector at each of the field points [37]. For instance, vortex Poynting singularities [91] are the points, around which circulation of the transverse component of the Poynting vector takes place. In other words, one deals here with the points which are the intersections of the observation plane and the axis of the angular momentum. Thus, spatial distributions of characteristics of the time-averaged Poynting vector components would contain important information on the field, which is concerned with the energy flows [24, 30, 35, 36].

Nevertheless, one can state that no the technique for experimental analysis of the time-averaged Poynting vector components and their singularities has been developed up to now. Here we would like to demonstrate that the components of the time-averaged Poynting vector can be experimentally analyzed by using conventional optical methods.

It has been shown [37, 87] that the instantaneous components of the Poynting vector may be written as

$$\begin{cases} P_x \approx \dfrac{c}{4\pi k}\{E_x T_2 - E_y T_1\}; \\ P_y \approx \dfrac{c}{4\pi k}\{E_y T_2 + E_x T_1\}; \\ P_z \approx \dfrac{c}{4\pi}\{E_x^2 + E_y^2\}, \end{cases} \tag{14}$$

where

$$\begin{cases} T_1 = E_x\Phi_x^y \quad E_y\Phi_y^x + \dfrac{A_x^y}{A_x}E_{x,\frac{\pi}{2}} - \dfrac{A_y^x}{A_y}E_{y,\frac{\pi}{2}}; \\ T_2 = E_x\Phi_x^x + E_y\Phi_y^y + \dfrac{A_x^x}{A_x}E_{x,\frac{\pi}{2}} + \dfrac{A_y^y}{A_y}E_{y,\frac{\pi}{2}}, \end{cases} \tag{15}$$

$$\begin{cases} E_i = A_i\cos(\omega t + \Phi_i - kz); \\ E_{i,\frac{\pi}{2}} = A_i\sin(\omega t + \Phi_i - kz), \end{cases} \tag{16}$$

$i = x, y$, A_i, Φ_i – denote, respectively, amplitudes and phases of the corresponding field components, A_i^l, Φ_i^l are their partial derivatives, and $k = \omega / c$ represents the wave number. Note, here the axis z coincides with the preferential direction of the wave propagation.

One can show after some algebraic transformations that the averaged components of the Poynting vector are as follows:

$$\begin{cases} \overline{P}_x \approx \dfrac{c}{8\pi k}\{[A_x^2\Phi_x^x + A_y^2\Phi_y^x] \quad A_xA_y(\Phi_x^y \quad \Phi_y^y)\cos\Delta - (A_xA_y^y + A_yA_x^y)\sin\Delta]\}; \\ \overline{P}_y \approx \dfrac{c}{8\pi k}\{[A_x^2\Phi_x^y + A_y^2\Phi_y^y] + A_xA_y(\Phi_x^x \quad \Phi_y^x)\cos\Delta + (A_xA_y^x + A_yA_x^x)\sin\Delta]\}; \\ \overline{P}_z \approx \dfrac{c}{8\pi}\{A_x^2 + A_y^2\}. \end{cases} \tag{17}$$

The second and the third terms in the brackets appearing of the first two rows of Eq. (17) may be rewritten as follows:

$$A_xA_y(\Phi_x^i - \Phi_y^i)\cos\Delta + (A_xA_y^i + A_yA_x^i)\sin\Delta = \frac{\partial}{\partial i}(A_xA_y\sin\Delta), \tag{18}$$

where $i = x, y$. Then, the system of Eqs. (17) is transformed to

$$\begin{cases} \overline{P}_x \approx -\dfrac{c}{8\pi k}\{[A_x^2\Phi_x^x + A_y^2\Phi_y^x] - \dfrac{\partial}{\partial y}(A_xA_y\sin\Delta)\} \\ \overline{P}_y \approx -\dfrac{c}{8\pi k}\{[A_x^2\Phi_x^y + A_y^2\Phi_y^y] + \dfrac{\partial}{\partial x}(A_xA_y\sin\Delta)\} \\ \overline{P}_z \approx \dfrac{c}{8\pi}\{A_x^2 + A_y^2\} \end{cases} \tag{19}$$

As it follows from Eqs. 19, one of the possible ways of the Poynting vector components measurement is complete analysis of orthogonal components:

Measurement of the components intensities (for the defining of components amplitudes and their corresponding derivatives).

Phasometry (interferometry) of the components (for the defining of components phases and their corresponding derivatives).

However, the phase difference between orthogonal components Δ is included in relations (19). Note that:

i. as it is known [17] measurement of the "absolute" phase in optics is "problematic". Only phase difference between object wave and referent one is fixed. In other words, the phase is measured within the constant component.
ii. the experimental arrangement for simultaneous measuring of component phase with the same constant components is practically impossible.

Consequently, the phase difference Δ cannot be measured within the enough accuracy by the components analysis. Such value may be easily measured by the Stokes polarimetry [83]. Stocks parameters for monochromatic wave have the form [17]:

$$\begin{aligned} s_0 &= A_x^2 + A_y^2 \\ s_1 &= A_x^2 - A_y^2 \\ s_2 &= 2A_x A_y \cos\Delta \\ s_3 &= 2A_x A_y \sin\Delta. \end{aligned} \tag{20}$$

Value Δ may be determined as:

$$\Delta = \tan^{-1}\frac{s_3}{s_2}, \tag{21}$$

and the Eqs. 19 may be used for the analysis of Poynting vector components. If one takes into account Eqs. (20), the relations (19) are transformed to the form:

$$\begin{cases} \overline{P}_x \approx -\dfrac{c}{16\pi k}\{[(s_0+s_1)\Phi_x^x + (s_0-s_1)\Phi_y^x] - \dfrac{\partial s_3}{\partial y}\} \\ \overline{P}_y \approx -\dfrac{c}{16\pi k}\{[(s_0+s_1)\Phi_x^y + (s_0-s_1)\Phi_y^y] + \dfrac{\partial s_3}{\partial x}\} \\ \overline{P}_z \approx \dfrac{c}{8\pi}s_0 \end{cases} \tag{22}$$

Thus, components of the Poynting vector may be defined by the Stokes parameters and derivatives of components phases. Note, that phasometry of only one component (let us y-component for certainty) is necessary, because a phase of the orthogonal component is determined as $\Phi_x = \Delta + \Phi_y$. Obviously, in practical sense, the phasometry of the smooth component (without any singularity in the analyzed area) is preferable.

As it is known (see, for example, [92] which is the closest for the topic of our study), three kinds of measurement are necessary for defining of phase of scalar field at each field point:

Intensity of component field $I_i = A_i^2$.

Intensity of referent wave $I_r = A_r^2$.

Intensity of total field I_s.

The component phase (within the constant component) may be derived from the relation:

$$\Phi_i = \arccos \frac{I_s - (I_i + I_r)}{2\sqrt{I_i I_s}}. \tag{23}$$

Naturally, the phase derivatives Φ_i^k, included in Eqs. (19), (22) are independent on the constant component.

Thus, joint applying of the conventional interferometry and Stokes-polarimetry allow us unambiguously determine the characteristics of the Poynting vector components at each point of an optical field.

6. Complex degree of mutual polarization of laser fields formed by birefringent matrices of biological tissues. Polarimetric metrology in diagnostics of structure and physiological state of biological tissues

Optical diagnostics of complex, inhomogeneous in phase objects, such as biological tissue (BT) includes relatively independent directions, *viz.* photometric, polarimetric and correlation. On the base of these directions, *laser polarimetry of BTs* has been formed as a new and intensively developed branch of applied optics metrology [93 - 97]. Within this branch, one considers morphological structure of BTs as two-component amorphous-crystalline structure. Crystalline component or extracellular matrix of BTs of the main types is formed by the net of coaxial cylindrical protein fibrils possessing the properties of uniaxial bireringent crystals.

Laser polarimetry has been shown to be efficient tool under single-scattering regime for finding out the set of interconnections among statistical (the first to the fourth statistical moments) and fractal (log-log dependence of power spectra) parameters, which characterize coordinate geometrical-optical structure of extracellular matrix of BT, on the one hand, and polarization parameters (coordinate distributions of the azimuth of polarization and ellipticity) at its image, on the other hand. The mentioned success in diagnostic application of laser polarimetry of optically thin BT layers stipulates further development of new statistical approaches for analysis of concordance of the states of polarization at various points of an object field formed by multy-layer BT, in part by applying the concepts of the complex degree of mutual polarization (CDMP) [6, 32, 98, 99] and determining on this base the complex degree of mutual anisotropy [100] of polycrystalline protein nets. It is of vital importance for development of new techniques for reliable estimating physiological state of optically anisotropic BTs.

Spatial modulation of correlation and polarization characteristics is intrinsic to laser radiation scattered by object fields, including images of BTs [4, 5, 93, 101 - 103]. Optical coherent tomography [104, 105] and its new branch, polarization-sensitive optical coherent tomography [95, 96, 101, 106, 107], are among the most promising techniques for obtaining information on such modulation. This diagnostic technique is based on measuring coordinate distributions of the Stokes parameters at BT images that give a possibility to obtain important data both on BT's microstructure and on magnitude and coordinate distribution of optical anisotropy of architectonic nets formed by birefringent protein fibrils. Further progress of polarization-sensitive optical coherent tomography presumes development of new techniques for polarimetric, interferometric and correlation analysis and processing of inhomogeneous in polarization images of BTs. Let us consider these techniques in more details.

6.1 Polarimetric approach

Laser radiation, similarly to natural light, can be absorbed and scattered by BT. Each of these processes leads to enrichment of the field by information on micro- and macrostructure of the studied medium and its components. Spectrophotometric techniques are among the most widely used now for diagnostics of BTs. These techniques are based on the analysis of spatial and temporal changes of intensity of a field scattered by optically inhomogeneous samples. At the same time, other diagnostic techniques are also intensively developed, being based on fundamental concepts of *polarization* and *coherence*.

Spatial fluctuations of the parameters of optical fields are traditionally characterized in terms of the field's coherent properties [1]. The concept of *the measure of coherence* between two light disturbances is associated with ability of such disturbances to produce interference pattern and, consequently, with visibility of an interference pattern [17, 108]. It is just the measure of the sum of correlations between equal polarization projections of electrical fields at two specified ponts.

Another type of correlation characteristics of scattered laser fields is the degree of polarization defined as the maximal magnitude of correlations between the orthogonal polarization projections of a field at the fixed point [17]. Polarization properties of a field are experimentally investigated by measuring intensity of radiation passed various optically active elements of a medium. The techniques based on the use of the coherency matrix and the degree of polarization related to correlation of orthogonal in polarization components at one point of a field are often referred to as the polarization techniques [93].

Intense development of vector (polarization) approach in the study of morphological structure and physiological state of various BTs [96] formed the basis for elaborating model concepts on optically anisothropic and self-similar structure of BTs [98, 109 - 112]. So, Cowin [113] analyzes hierarchical self-similar structure of typical connective tissue, *viz.* tendon (tropocollagen, microfibril, subfibril, fascia etc.) Cowin emphasizes that threadlike structural elements are discrete, being characterized by scale recurrence over large interval of "optical sizes" (from 1 μm to 10^3 μm). For that, optical characteristics of such structure of BT correspond, generally, to "frozen" optically uniaxial liquid crystals.

The same approach for describing morphological structure of BT has been applied in Refs [111, 112], where a BT is considered as two-component amorphous-crystalline structure. Amorphous component of BT (fat, lipids, unstructured proteins) is isotropic in polarization, i.e. optically inactive.

Crystalline component of BT is formed by oriented birefringent protein fibrils (collagen proteins, myosin, elastin etc.). The properties of the each isolated fibril are modeled by optically uniaxial crystal, whose axis direction coincides with the direction of packing at the plane of BT, and the birefringence coefficient is determined by the fibril matter. Architectonic net formed by disordered birefringent fibrils constitutes higher level of BT organization.

This model provides explanation of polarization inhomogeneity of object fields produced by BTs of various types, such as osseous and muscular tissues, tissues of female reproductive organs (myometrium) [111, 112]. The interconnections between the azimuth of polarization and ellipticity of a field, on the one hand, and the directions of packing of fibrils, as well as

the parameters characterizing birefringence, on the other hand, have been also determined for the single-scattering regime [113]. It allowed improving the technique of polarization visualizing the BT's architectonics by applying statistical analysis of 2D distributions of scattered fields [111, 112].

The papers [111, 114, 115] represent the results on determining the interconnections among the set of the 1st to the 4th order statistical moments characterizing microgeometry of a surface and orientation/phase structure of human BT's birefringent architectonics, on the one hand, and the set of the corresponding statistical moments of 2D distributions of the azimuth of polarization and ellipticity of the images of these objects, i.e. polarization maps, on the other hand. It has been stated that increasing asymmetry and excess characterizing the distributions of the azimuth of polarization and ellipticity at polarization maps result from increasing dispersion in orientation of birefringent fibril optical axes. Decreasing asymmetry and excess correspond to increasing dispersion of phase delays caused by biological crystals of architectonic nets.

Further development of laser polarimetry led to new techniques for measuring 2D arrays of polarization parameters that characterize nets of biological crystals inherent in various types of human's BTs. So, statistical analysis of the coordinate distributions of the Stokes parameters provide new information on microstructure (such as magnitudes and coordinate distributions of the parameters of optical anizotropy of architectonic nets formed by collagen or myosin) of physiologically normal and pathologically changed BTs [116]. Generally, intensive development of the techniques for diagnostic applications of laser radiation has been reflected into optical coherent tomography that became the most elaborated and convenient instrument for non-invasive study of BT structure.

The use of polarization of laser beam as a tool for contrasting of BT images resulted in a new branch of optical coherent tomography (OCT) [94, 104, 105], *viz.* polarization-sensitive optical coherent tomography (PSOCT) [95, 96, 101, 106, 107]. Note, special feature of *laser polarimetry of distributions of the azimuth of polarization and ellipticity* consists in point-by-point analysis of the object field's polarization parameters followed by searching for interconnections of these parameters with orientation and anisotropic parameters of BT's architectonics. For that, it leaves undetermined the data on peculiarities (statistical, fractal) of 2D distributions of polarization parameters of a field and orientation/phase characteristics of an object. So, further development of the techniques for non-invasive macro-diagnostics of geometrical optical structure of BT through improving conventional polarization-interference mapping and looking for new techniques for reconstruction of BT architectonics is among vital topics of modern optics.

6.2 Optical correlation approach

It is known [5, 32, 98, 108] that polarization properties of light at specified point of space can be described by the coherency matrix. This formalism is comprehensive for of a light field as a whole, when the field in statistically homogeneous, i.e. when the field's characteristics are independent on spatial coordinates. However, for spatially inhomogeneous fields it is of importance to know not only coordinate distributions of polarization parameters, but also interconnections of the states of polarization and the degree of coherence at different points of a field.

The first attempt to describe spatially inhomogeneous in polarization optical fields consisted in direct generalization of the coherency matrix to the two-point coherency (polarization) matrix performed by Gori [98, 117]. (Note, this principle of representation of optical fields of general type, i.e. partially spatially coherent and inhomogeneously polarized fields, even without restrictions connected with the paraxial approximation, has been explicitly formulated yet at the morning of the era of lasers (*'litic age'*), in the early sixties, being summed up in seminal review by Wolf and Mandel [1].) In *'post-litic age'*, Gori shows that some magnitude of interference pattern's visibility corresponds to the each coherency matrix element; these patterns result from superposition of radiations from two point sources whose polarization characteristics are formed by the set of polarizers and phase plates. Matrix analysis of correlation properties of scattered coherent radiation has been generalized for vector (inhomogeneously polarized) fields [109, 110].

As much prospective is the development of the tools for direct measuring CDMP in problems of biomedical optics connected with processing of coherent, inhomogeneous in polarization images of BTs obtained by allying the OCT techniques. It has been shown [100] that the CDMP of BT's coherent image is the parameter sensitive to orientation/phase changes of BT's architectonics. Experimental study [118] of 2D distributions of the CDMP of BT's laser images for examples of muscular, skin and osseous tissues have corroborated existence of the interconnections between the coordinate structure of the CDMP at laser images and geometrical/optical structure of birefingent architectonic nets of physiologically normal and dystrophycally changed BTs. Taking into account diagnostic feasibilities of the CDMP, further searching for peculiarities of the coordinate distributions of this parameter for various BTs seems to be quite relevant and urgent problem. The following consideration is devoted to this problem.

6.3 BT as birefringent extracellular matrix transforming laser light parameters

As it has been mentioned above, BT consists of two components, *viz*. optically isotropic (amorphous) and anisotropic net (extracellular matrix) of birefringent optically uniaxial fibril [4, 94, 103, 111, 112], see Figure 20.

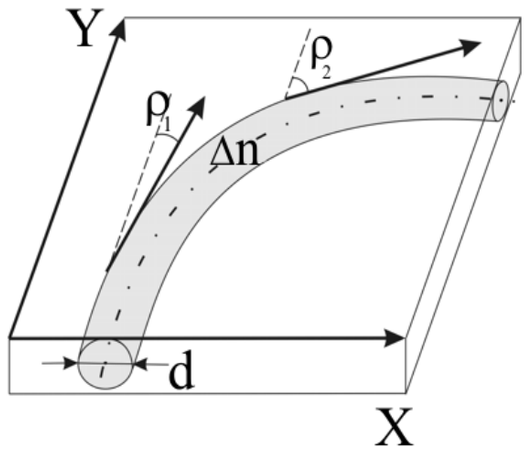

Fig. 20. Δn - d-diam birefringent fibril; ρ_i - the directions of the fibril packing at the plane of a BT sample.

The action of amorphous and architectonic (crystalline) components of BT, $\{A\}$ and $\{C\}$, respectively, on coherent radiation is characterized by the following Jones matrix operators:

$$\{A\} = \begin{Vmatrix} a_{11} & a_{12} \\ a_{21} & a_{22} \end{Vmatrix} = \begin{Vmatrix} \exp(-\tau l) & 0 \\ 0 & \exp(-\tau l) \end{Vmatrix}; \tag{24}$$

$$\{C\} = \begin{Vmatrix} c_{11} & c_{12} \\ c_{21} & c_{22} \end{Vmatrix} = \begin{Vmatrix} \cos^2\rho + \sin^2\rho\exp(-i\delta); & \cos\rho\sin\rho\left[1-\exp(-i\delta)\right]; \\ \cos\rho\sin\rho\left[1-\exp(-i\delta)\right]; & \sin^2\rho + \cos^2\rho\exp(-i\delta); \end{Vmatrix} \tag{25}$$

Here, τ is the absorption coefficient for BT of thickness l; ρ is the packing direction of anisotropic fibril (with birefringence coefficient Δn) at the plane of a BT's sample introducing a phase shift $\delta = 2\pi/\lambda\,\Delta n l$ between the orthogonal polarization components, E_x, E_y, of the probing laser beam of wavelength λ.

6.4 Mechanisms of forming inhomogeneous in polarization BTs laser images

As it follows from analysis performed in Refs [93, 95, 97, 113] the mechanism of forming inhomogeneous in polarization boundary field of a BT at each point can be represented in the following form:

"decomposition" of an amplitude of laser wave U into orthogonal linearly polarized mutually coherent components:

$$\begin{pmatrix} U_x(r) \\ 0 \end{pmatrix} \text{ and } \begin{pmatrix} 0 \\ U_y(r) \end{pmatrix};$$

forming a phase shift (phase difference) between these components accounting birefringence, $\delta(r)$;

superposing the orthogonally polarized components that results, in general case, in elliptically polarized wave that is described by the following equation:

$$\frac{X^2}{U_x^2(r)} + \frac{Y^2}{U_y^2(r)} - \frac{2XY}{U_x(r)U_y(r)}\cos\delta(r) = \sin^2\delta(r)\,. \tag{26}$$

6.5 Statistical and fractal analysis of polarization images of BTs

Two types of optically thin (extinction coefficient $\tau \le 0.1$) of BT's histological tomes have been studied in Refs [4, 97]:

- structured osseous tissue (Fig. 21 a, b);
- parenchymatous tissue of kidney (Fig. 21 c, d).

Coordinate distributions $\{\alpha(r);\beta(r)\}$ and histograms $W(\alpha), W(\beta)$ of the magnitudes of the azimuth of polarization and ellipticity at images of histological tomes of physiologically normal osseous tissue (left part) and kidney tissue (right part) are shown in Figure 22 (fragments (a), (b) and (c), (d), respectively).

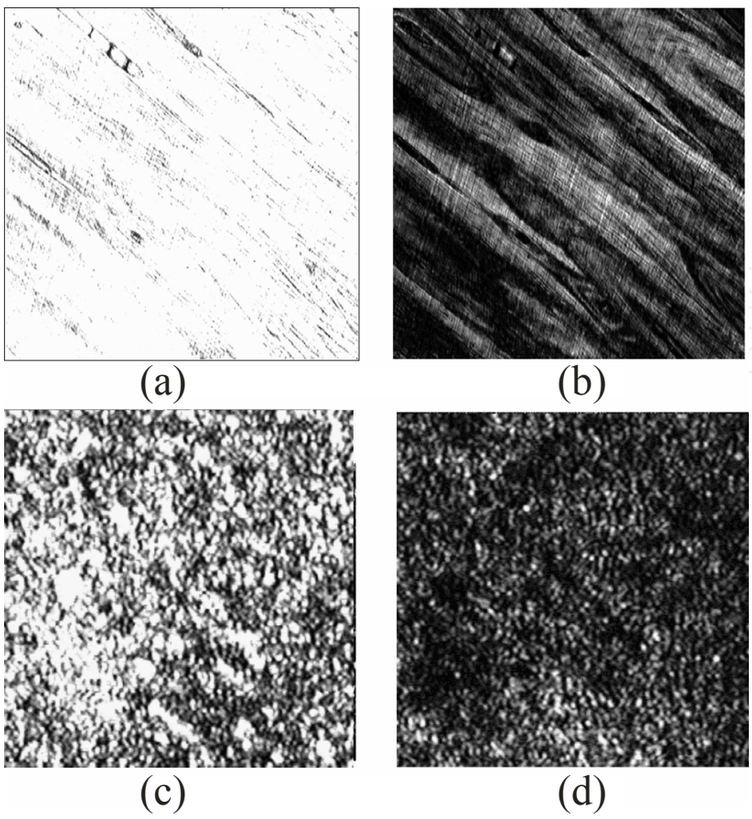

Fig. 21. Polarization images of osseous tissue (a, b) and tissue of kidney (c, d) for matched (a, c) and crossed (b, d) polarizer and analyzer, respectively.

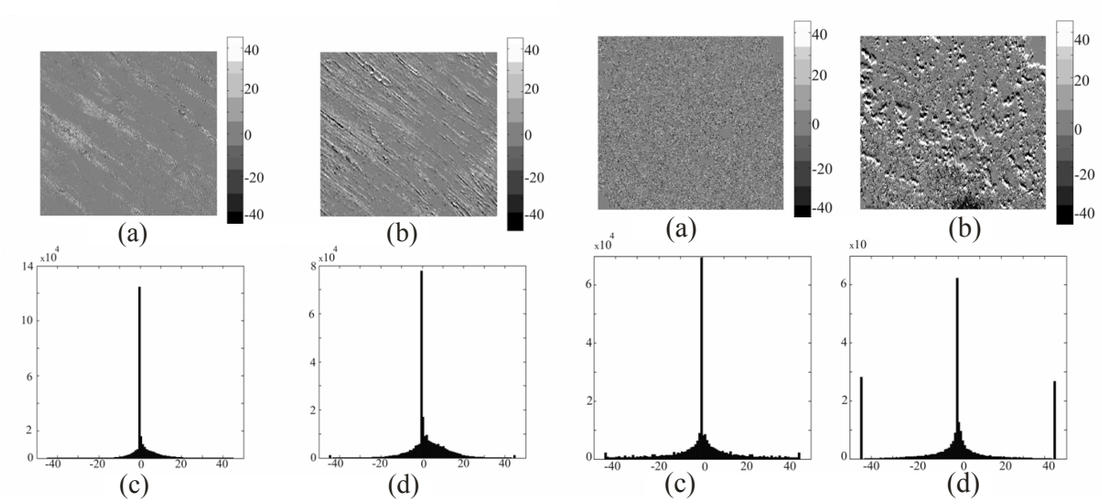

Fig. 22. Polarization maps of osseous tissue (left part) and kidney tissue (right part). Fragments (a), (b) correspond to 2D distributions of the azimuth of polarization and ellipticity, respectively; fragments (c), (d) show histograms of the corresponding distributions.

Distributions of the azimuth of polarization and ellipticity of the maps of BTs of two types characterize the set of statistical moments of the 1st to the 4th orders shown in Table 1.

The obtained data for statistical moments of the 1st to the 4th orders for distributions $W(\alpha), W(\beta)$ of images of BTs of different morphological construction show that as birefringent architectonic nets are higher structured, as the magnitudes of the 3rd and the 4th statistical moments associated with the set of polarization parameters increase.

	Osseous tissue (31 samples)				*Kidney tissue (27 samples)*		
	$\alpha(r)$		$\beta(r)$		$\alpha(r)$		$\beta(r)$
M_1	$0{,}38 \pm 0{,}027$	M_1	$0{,}24 \pm 0{,}014$	M_1	$0{,}11 \pm 0{,}01$	M_1	$0{,}08 \pm 0{,}004$
M_2	$0{,}25 \pm 0{,}015$	M_2	$0{,}21 \pm 0{,}017$	M_2	$0{,}19 \pm 0{,}013$	M_2	$0{,}05 \pm 0{,}003$
M_3	$9{,}8 \pm 0{,}882$	M_3	$7{,}7 \pm 0{,}539$	M_3	$1{,}4 \pm 0{,}056$	M_3	$0{,}61 \pm 0{,}04$
M_4	$24{,}6 \pm 2{,}71$	M_4	$12{,}5 \pm 1{,}125$	M_4	$3{,}1 \pm 0{,}093$	M_4	$2{,}25 \pm 0{,}113$

Table 1. Statistical momentums M_i of the coordinate distributions of the states of polarization at images of BTs of osseous and kidney BTs

6.6 Diagnostic feasibilities of polarization mapping of optically thin layers of BTs

To look for the feasibilities for differentiation of geometrical/optical structure of architectonics of BTs, comparative study of statistical and fractal structures of BT maps has been carried out [103, 119 - 121]. There are BTs of interest: (i) physiologically normal and dystrophically changed muscular tissue (MT), i.e. structured BT with ordered architectonics; (ii) physiologically normal and septically inflamed pulmonary tissue (PT), i.e. BT with island architectonics. The set of figures (Figs. 23 and 24) illustrates polarization maps of the mentioned objects.

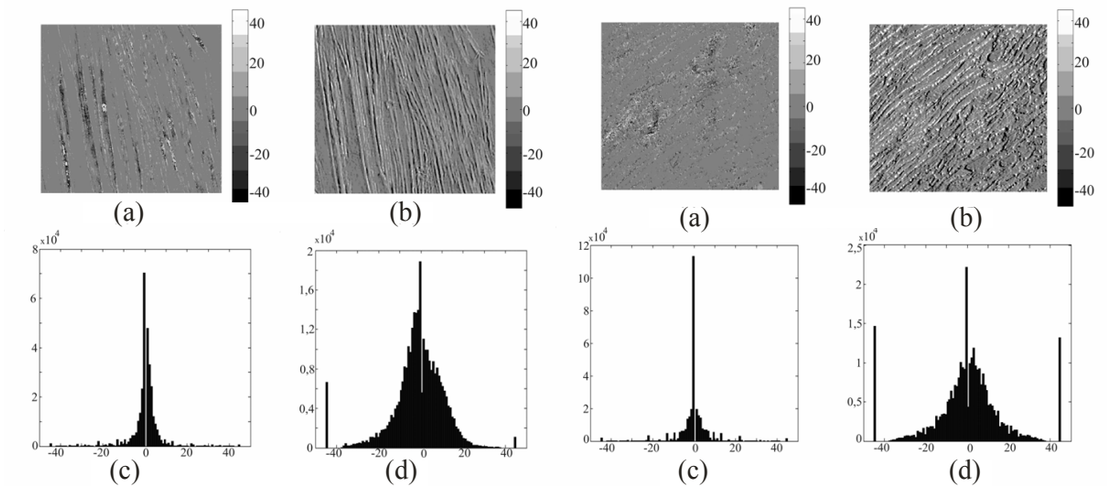

Fig. 23. Polarization maps of physiologically normal (left part) and dystrophycally changed (right part) MT: (a), (b) – 2D distributions (in degrees) of the azimuth of polarization and ellipticity; (c), (d) – histograms of polarization parameters.

Potentialities for statistical differentiation of polarization maps are illustrated by comparison of magnitudes of the statistical moments of the 1st to the 4th orders for the azimuth of polarization and ellipticity at images of physiologically normal and pathologically changed BTs, represented in Tables 2 and 3.

	Norm (21 samples)			*Pathology (22 samples)*	
M_1	α	β	M_1	α	β
M_1	*0,26 ± 0,013*	*0,12 ± 0,01*	M_1	*0,21 ± 0,001*	*0,18 ± 0,011*
M_2	*0,12 ± 0,01*	*0,08 ± 0,004*	M_1	*0,19 ± 0,013*	*0,12 ± 0,006*
M_3	*6,7 ± 0,469*	*4,9 ± 0,294*	M_1	*9,4 ± 0,846*	*6,2 ± 0,434*
M_4	*17,9 ± 1,61*	*14,5 ± 1,595*	M_1	*25,4 ± 2,54*	*21,6 ± 2,592*

Table 2. Statistical moments of the 1st to the 4th orders for the coordinate distributions of the azimuth of polarization and ellipticity at images of histological tomes of normal and dystrophically changed MT

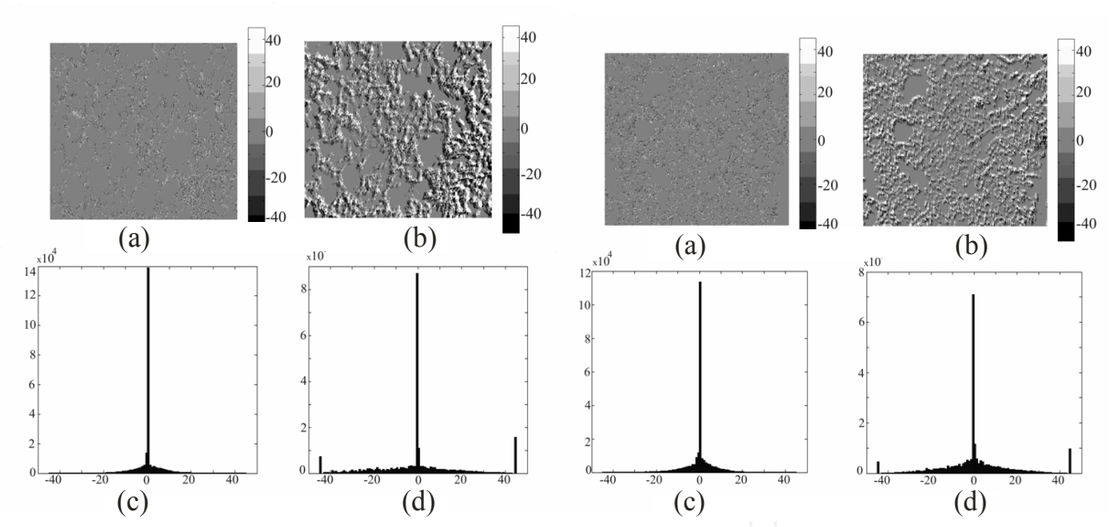

Fig. 24. Polarization maps of physiologically normal (left part) and septically inflamed (right part) PT: (a), (b) – 2D distributions (in degrees) of the azimuth of polarization and ellipticity; (c), (d) – histograms of polarizarion parameters.

One can see from the represented data that magnitudes of asymmetry and excess of the coordinate distributions of the azimuth of polarization and ellipticity at BT images with ordered architectonics (Table 2) exceed by 3 to 5 times the magnitudes of the corresponding parameters characterizing statistics of the 3rd and the 4th orders of inhomogeneous in polarization BT images with island architectonics (Table 3).

	Norm (22 samples)			*Pathology (22 samples)*	
M_1	α	β	M_1	α	β
M_1	*0,08 ± 0,004*	*0,06 ± 0,004*	M_1	*0,09 ± 0,004*	*0,08 ± 0,005*
M_2	*0,19 ± 0,013*	*0,16 ± 0,02*	M_2	*0,21 ± 0,01*	*0,2 ± 0,016*
M_3	*3,12 ± 0,25*	*2,64 ± 0,29*	M_3	*2,04 ± 0,184*	*1,18 ± 0,142*
M_4	*6,92 ± 0,76*	*2,17 ± 0,282*	M_4	*4,17 ± 0,5*	*7,28 ± 1,092*

Table 3. Statistical moments of the 1st to the 4th orders for the coordinate distributions of the azimuth of polarization and ellipticity at images of histological tomes of normal and septically inflamed PT

On the other hand, structured BTs possess hierarchical, self-similar structure of architectonics [97, 113, 120]. That is why one must determine optical manifestations of such geometry of anisotropic component of structured BTs. The study of self-similarity of polarization maps of BTs has been carried out for skin derma.

Figure 25 shows the set of log-log dependences, $\log P(\alpha) - \log(1/d)$, $\log P(\beta) - \log(1/d)$, for power spectra of the distributions of polarization parameters at images of physiologically normal and pathologically changed skin derma.

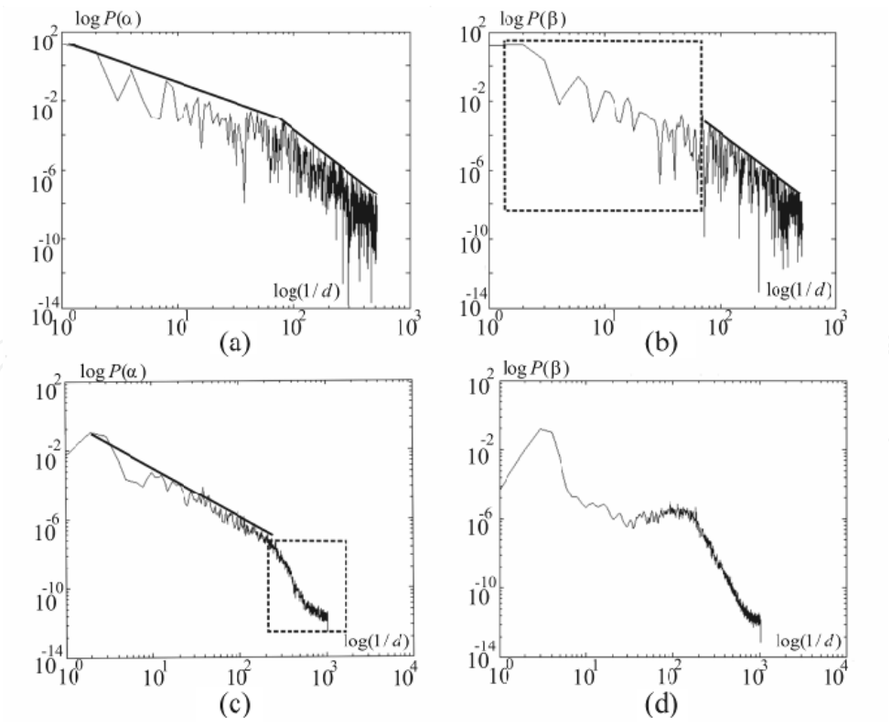

Fig. 25. log-log dependences of power spectra of the azimuth of polarization and ellipticity at images of physiologically normal (a), (b) and pathologically changed (c), (d) skin derma.

The dependence $\log P(\alpha) - \log(1/d)$ manifests two slopes within three decades of scales of architectonics of skin derma's elements; the dependence $\log P(\beta) - \log(1/d)$ consists of the part with constant slope and statistical part, as it is seen from Fig. 1.6 (a) and (b). Pathological state of such BT manifests itself in randomization of distributions of polarization parameters at images of the corresponding histological tomes, i.e. for approximating curves (Fig. 25 (c) and (d)) steady slope is absent.

6.7 Degree of mutual polarization of laser images of BTs

For laser light fields scattered by BTs, coordinate changes of polarization characteristics can be characterized by the complex degree of mutual polarization, CDMP, at two points $(r_1; r_2)$ [6]:

$$W(r_1, r_2) = \frac{\left(U_x(r_1)U_x(r_2) - U_y(r_1)U_y(r_2)\exp\left(i\left(\delta_2(r_2) - \delta_1(r_1)\right)\right)\right)^2}{\left(U_x^2(r_1) + U_y^2(r_1)\right)\left(U_x^2(r_2) + U_y^2(r_2)\right)}. \tag{27}$$

The following interconnections between the real part of the CDMP, $\mathrm{Re}W \equiv \bar{W}(r_1, r_2)$, and the magnitudes at the azimuth of polarization, $\alpha(r)$, ellipticity, $\beta(r)$, at points r of BT's image, and orthogonal components $U_x = \sqrt{I_x}, U_y = \sqrt{I_y}$ of the complex amplitude with phase difference between them $\delta(r)$ have been established in study [100]:

$$\bar{W}(r_2, r_1) = \frac{\left(\left(I_x(r_2)I_x(r_1)\right)^{\frac{1}{2}} - \left(I_y(r_2)I_y(r_1)\right)^{\frac{1}{2}}\cos\left(\delta_2(r_2) - \delta_1(r_1)\right)\right)^2}{I(r_2)I(r_1)}, \tag{28}$$

where

$$\delta(r_1) = \tan^{-1}\left[\frac{\tan\left[2\beta(r_1)\right]}{\tan\left[\alpha(r_1)\right]}\right]; \quad \delta(r_2) = \tan^{-1}\left[\frac{\tan\left[2\beta(r_2)\right]}{\tan\left[\alpha(r_2)\right]}\right]. \tag{29}$$

6.8 Statistical approach to analysis of coordinate distributions of the CDMP at BT images

Normal and dystrophycally changed tissues of skeleton muscle has been investigated in paper [100]. Coordinate distributions of the CDMP $\bar{W}(x, y)$ at images of histological tomes of such samples are shown in Figure 26.

Statistical analysis of the coordinate distributions of magnitudes $\bar{W}(x, y)$ shows for the map of tissue of skeleton muscle differences between the statistical moments of the 1st to the 3rd orders (within 30%-50%), while magnitudes of excess (the 4th order statistical moment) differ by 2 to 2.5 times.

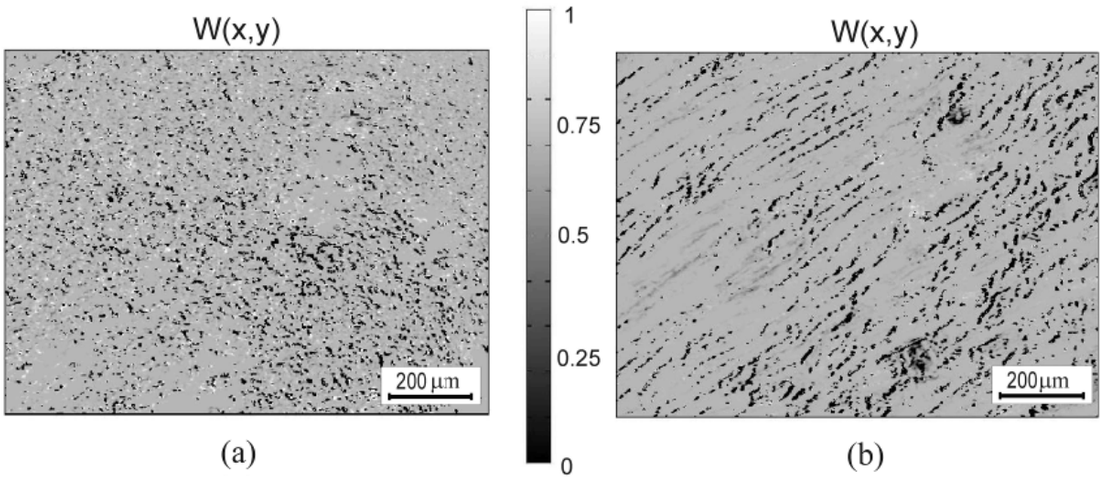

Fig. 26. Coordinate distributions of the CDMP at images of histological tomes of normal (a) and dystrophycally changed (b) tissue of skeleton muscle.

Statistical moment	*Muscular tissue (norm) 28 samples*	*Muscular tissue (pathology) 25 samples*
M_1	*0,62 ± 0,03*	*0,49 ± 0,02*
M_2	*0,1 ± 0,06*	*0,14 ± 0,01*
M_3	*32 ± 3,2*	*21 ± 2,31*
M_4	*81 ± 8,72*	*43 ± 3,87*

Table 4. Statistical moments of the 1st to the 4th orders for distributions of magnitudes $\bar{W}(x,y)$ at images of histological tomes of normal and dystrophically changed tissues of skeleton muscle.

Figure 27 shows autocorrelation functions of the coordinate distributions of magnitudes of the CDMP at images of histological tomes of samples of normal (a) and pathologically changed (b) muscular tissues.

Parameter	*Muscular tissue*	
	Norm	*Pathology*
L	*0,25 ± 0,02*	*0,13 ± 0,01*
Ω	*0,07 ± 0,005*	*0,005 ± 0,0001*

Table 5. Correlation parameters of the distributions of the CDMP, $\bar{W}(x,y)$, for normal and pathologically changed osseous muscular tissues.

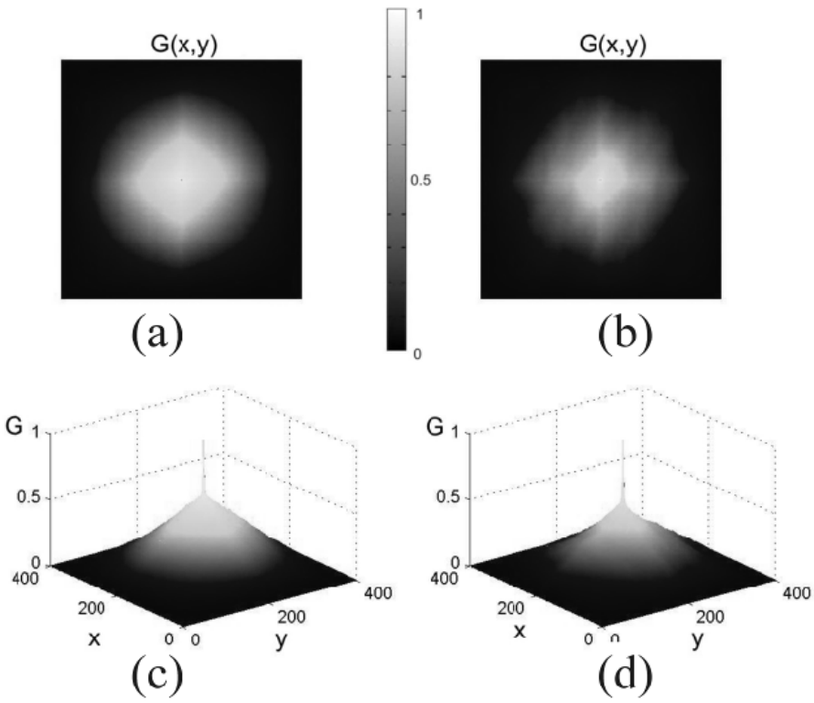

Fig. 27. Autocorrelation functions $G(x,y)$ of 2D distributions of the CDMP, $\bar{W}(x,y)$, at images of histological tomes of muscular tissues.

Correlation analysis of 2D distributions of magnitudes $\bar{W}(x,y)$ leads to the following conclusions: (*i*) differences between magnitudes of a half-width L of autocorrelation functions for distributions $\bar{W}(x,y)$ at polarization/correlation maps of muscular tissue's maps are within the interval 0.65 to 2 times; (*ii*) differences between dispersions of the distributions for extrema of power spectra for $\bar{W}(x,y)$ reach one order of magnitude.

Thus, the analysis of approaches and metrological techniques of modern polarimetric diagnostics of birefringent nets of BTs leads to the following conclusions.

- higher-order statistical moments (asymmetry and excess) characterizing the distributions of polarization/correlation parameters of laser images of BTs are of the highest sensitivity in respect to changing optical properties of nets of biological crystals of normal and pathologically changed BTs;
- interconnection between the real part of the CDMP and parameters of anisotropy (such as direction of an optical axis and phase difference between orthogonal components of scattered laser radiation) at different points of birefringent matrix provides reliable tool for correlation optical diagnostics of pathological changes of biological tissues and, as a consequence, for early and non-invasive diagnostics of wide-spread diseases, which challenge Humanity in the Third Millenium.

7. Conclusions

Thus, new approaches to metrology of partially coherent and partially polarized light fields are derived proceeding from singular optics concept. The first of them concerns to exploring

the spatial modulated time-averaged Poynting vector in completely and partially coherent non-paraxial light fields for control the motion of nano- and microparticles in optical currents. The second approach reveals interconnection between polarization singularities inherent in completely polarized and partially polarized optical beams for the general case of partially mutual coherence of orthogonally polarized components. Further, we have shown the feasibility for experimental analysis of the Poynting vector components by combining interferometric and polarimetric metrological techniques. At last, we have demonstrated potentialities of laser 2D Stokes-polarimetric metrological technique developed and implemented in previous consideration in non-invasive pre-clinic diagnostics of physiological state of biological tissues. The represented approaches show fruitfulness of attracting the concepts and metrological tools of singular optics in formation and investigation of unconventional polarization distributions that can be of usefulness in problems of optical correlation diagnostics and optical telecommunications.

There are the important next steps in developing the direction of Metrology represented in this chapter. The study of optical currents using light-scattering particles of nano-scale will provide vital data both on microstructure of light and on intimate processes of interaction of optical beams with extremely small (in scale of a wave length) particles and ensembles of them. It is in prospect to investigate experimentally in more details influence of varying degree of coherence of optical fields on some phenomena considered in this review and associated with peculiarities (*singularities*) of the Poynting vector in complex inhomogeneous optical fields beyond the paraxial approximation. Also, it is important to obtain experimental verification, *viz*. visualization, of the mechanical action of the spin moment in optical beams. The study of influence of polarization characteristics of light field on motion of nanoparticles will be continued, as well as development of biomedical application of notion and techniques of completely/partially coherent, inhomogeneously polarized fields.

Another branch of the following R&D must be focused, in our opinion, on overcoming some disadvantages intrinsic to digital optical data surveying due to automatic gain control applied in the most of register tools, including CCD cameras. Really, dealing with differentiation metrology (such as 2D Stokes polarimetry) one wants to have comparable data in the set of measurements that is not always achievable with self-controlled in sensitivity digital registering devices. As compromise, one can consider combination of analog data recording and digital processing of these data. Nevertheless, this important point is worthy separate investigation for providing higher accuracy and reliability of modern optical metrology.

8. Acknowledgement

This work was supported by the Ministry of Education and Science of Ukraine, Grants No 0110U000188 and No 0111U000719.

9. References

[1] Wolf, E. & Mandel, L. (1965). Coherence properties of optical fields, Rev. Mod. Phys. V. 37, (1965), pp. 231-287

[2] Soskin, M.S. & Vasnetsov, M.V. (2001). Singular Optics, In: *Progress in Optics*, Wolf, E., V. 42, (2001), pp. 219–276
[3] Gbur, G. & Visser, T.D. (2010). The Structure of Partially Coherent Fields, In: *Progress in Optics*, Wolf, E., V. 55, Issue C, (2010), pp. 285-341
[4] Angelsky, O.V.; Ushenko, A.G.; Ushenko, Yu.A. & Pishak, V.P. (2007). Statistical and Fractal Structure of Biological Tissue Mueller Matrix Images, In: *Optical Correlation Techniques and Applications*, Angelsky, O.V., pp. 213-266, Washington: Society of Photo-Optical Instrumentation Engineers
[5] Wolf, E. (2003). Unified theory of coherence and polarization of random electromagnetic beams, *Phys. Lett. A,* V. 312, (2003), pp. 263-267
[6] Ellis, J. & Dogariu, A. (2004). Complex degree of mutual polarization, *Opt. Lett.* V. 29, (2004), pp. 536-538
[7] Mandel, L. (1998). Anticoherence, Pure Appl. Opt. V. 7, (1998), pp. 927-932
[8] Collier, R.; Burckhardt, L. & Lin, L. (1971). *Optical Holography*, Academic, New York
[9] Goodman, J.W. (1985). *Statistical Optics*, Wiley-Interscience, New York
[10] Glauber, R.J. (1962). *Lectures in Theoretical Physics* (4), Brittin, W.E.; Downs, J. (Eds.) Interscience, New York
[11] Glauber, R.J. (1963). The quantum theory of optical coherence, *Phys Rev.* V. 6, (1963), pp. 2529-2539
[12] Glauber, R.J. (1965). Optical Coherence and Photon Statistics, In: *Quantum Optics and Electronics*, deWitt, C.; Blandin, A. & Cohen-Tannoudji, C., pp. 65–185, Gordon & Breach, New York
[13] Dirac, P.A.M. (1985). *Principles of Quantum Mechanics*, (4), Oxford U. Press, Oxford
[14] Wolf, E. (1987). Non-cosmological redshifts of spectral lines, *Nature,* V. 326, (1987), pp. 363-365
[15] Wolf, E. & James, D.F.V. (1996). Correlation-induces spectral changes, *Rep. Progr. Phys.*, V. 59, (1996), pp. 771-818
[16] Polyanskii, V.K. & Kovalskii, L.V. (1973). On fine structure of the scattered radiation field, *Opt. Spectrosc.*, V. 35, (1973), pp. 345-350
[17] Born, M. & Wolf, E. (1999). *Principles of Optics*, (7), (expanded), Cambridge U. Press, Cambridge
[18] Nye, J.F. (1999). *Natural Focusing and Fine Structure of Light: Caustics and Wave Dislocations* Institute of Physics Publishing, Bristol and Philadelphia
[19] Freund, I. (2004). Coherency matrix description of optical polarization singularities, *J. Opt. A: Pure Appl. Opt.*, V. 6, (2004), pp. 229-234
[20] Dolgov, A.D.; Doroshkevich, A.G.; Novikov, D.I. & Novikov, I.D. (1999). Classification of singular points in the polarization of the cosmic microwave background and eigenvectors of the Stokes matrix, *JETP Lett.,* V. 69, (1999), pp. 427-433
[21] Hawking, S. (1988). *A Brief History of Time,* Bantam Press, ISBN 055305340X
[22] Van de Hulst, H.C. (1957). *Light Scattering by Small Particles*, Wiley, New York
[23] Bohren, C.F. & Huffman, D.R. (1983). *Absorbing and Scattering of Light by Small Particles*, Wiley, New York
[24] Berry, M.V. (2009). Optical currents, *J. Opt. A: Pure Appl. Opt*, V. 11, (2009), 094001
[25] He, H.; Friese, M.E.J.; Heckenberg, N.R. & Rubinsztein-Dunlop, H. (1995). Direct observation of transfer of angular momentum to absorbtive particles from a laser beam with a phase singularity, *Phys. Rev. Lett.*, V. 75, (1995), pp. 826-829

[26] Simpson, N.B.; Dholakia, K.; Allen, L. & Padgett, M.J. (1997). Mechanical equivalence of spin and orbital angular momentum of light: an optical spanner, *Opt. Lett.*, V. 22, (1997), pp. 52-54

[27] O'Neil, A.T.; MacVicar, I.; Allen, L. & Padgett, M.J. (2002). Intrinsic and extrinsic nature of the orbital angular momentum of a light beam, *Phys. Rev. Lett.*, V. 88, (2002), 053601

[28] Garces-Chavez, V.; McGloin, D.; Summers, M.D.; Fernandez-Nieves, A.; Spalding, G.C.; Cristobal, G. & Dholakia, K. (2004). The reconstruction of optical angular momentum after distortion in amplitude, phase and polarization, *J. Opt. A: Pure Appl. Opt.*, V. 6, (2004), pp. 235-238

[29] Khonina, S.N.; Kotlyar, V.V.; Skidanov, R.V.; Soifer, V.A.; Jefimovs, K.; Simonen, J. & Turunen, J. (2004). Rotation of microparticles with Bessel beams generated by diffractive elements, *J. Mod. Opt.*, V. 51, (2004), pp. 2167-2184

[30] Bekshaev, A.; Soskin, M. & Vasnetsov, M. (2008). *Paraxial Light Beams with Angular Momentum*, Nova Science Publishers, New York

[31] Friberg, A.; Gao, C.; Eppich, B. & Weber, H. (1997). Generation of partially coherent fields with twist, *Proc. of SPIE 1997,* V. 3110, pp. 317-328

[32] Tervo, J.; Setala, T. & Friberg, A. (2003). Degree of coherence for electromagnetic fields, *Opt. Express.*, V. 11, (2003), pp. 1137-1143

[33] Setala, T.; Tervo, J. & Friberg, A.T. (2004). Complete electromagnetic coherence in the space-frequency domain, *Opt. Lett.*, V. 29, (2004), 328330

[34] Tervo, J.; Setala, T. & Friberg, A.T. (2004). Theory of partially coherent electromagnetic fields in the space-frequency domain, *J. Opt. Soc. Am. A,* V. 21, (2004), pp. 2205-2215

[35] Bekshaev, A.Ya. (2009). Oblique section of a paraxial light beam: criteria for azimuthal energy flow and orbital angular momentum, *J. Opt. A: Pure Appl. Opt.,* V. 11, (2009), 094003

[36] Bekshaev, A.Ya.; Bliokh, K.Y. & Soskin, M.S. (2011). Internal flows and energy circulation in light beams, *J. Opt.*, V. 13 053001 (32pp) doi:10.1088/2040-8978/13/5/053001

[37] Angelsky, O.V. (Ed). (2007). *Optical Correlation Techniques and Applications*, TA 1630, A6, SPIE Press, Bellingham, Washington

[38] Angelsky, O.V.; Polyanskii, P.V. & Maksimyak, P.P. (2008). Speckles and Phase Singularities in Polychromatic Fields, In: *New Directions in Holography and Speckle*, Caulfield, H.J.; Vikram, Ch.S., pp. 37-53 (Chapter 3), Kluwer Academic Publishers, Boston

[39] Angelsky, O.V.; Dominikov, N.N.; Maksimyak, P.P. & Tudor, T. (1999). Experimental revealing of polarization waves, *Appl. Opt.*, V. 38, (1999), pp. 3112-3117

[40] Tudor, T. (1997). Polarization waves as observable phenomena, *J. Opt. Soc. Am. A,* V. 14, (1997), pp. 2013-2020

[41] Berry, M.V. & Donald, K.T. (2008). Exact and geometrical optics energy trajectories in twisted beams, *J. Opt. A: Pure Appl. Opt.*, V. 10, (2008), 035005

[42] Berry, M.V. & Dennis, M.R. (2001). Polarization singularities in isotropic random vector waves, *Proc . R. Soc.,* A. 456, (2001), pp. 2059-2079

[43] Angelsky, O.V.; Hanson, S.G.; Zenkova, C.Yu.; Gorsky, M.P. & Gorodyns'ka, N.V. (2009). On polarization metrology (estimation) of the degree of coherence of optical waves, *Opt. Expr.*, V. 17, (2009), pp. 15623-15634

[44] Zenkova, C.Yu.; Gorsky, M.P.; Maksimyak, P.P. & Maksimyak, A.P. (2010). Optical currents in vector fields, *Appl. Opt.*, V. 50, (2010), pp. 1105-1112

[45] Mujait, M.; Dogariu, A. & Wolf, E. (2004). A law of interference of electromagnetic beams of any state of coherence and polarization and the Fresnel-Arago interference laws, *J. Opt. Soc. Am.*, A 21, (2004), pp. 2414-2417

[46] Ellis, J.; Dogariu, A.; Ponomarenko, S. & Wolf, E. (2005). Degree of polarization of statistically stationary electromagnetic fields, *Opt. Commun.*, V. 248, (2005), pp. 333-337

[47] Khrobatin, R. & Mokhun, I. (2008). Shift application point of angular momentum in the area of elementary polarization singularity, *J. Opt. A: Pure Appl. Opt.*, V. 10, (2008), 064015

[48] Khrobatin, R.; Mokhun, I. & Victorovskaya, Ju. (2008). Potentiality of experimental analysis for characteristics of the Poynting vector components, *Ukr. J. Phys. Opt.*, V. 9, (2008), pp. 182-186

[49] Bekshaev, A.Ya. & Soskin, M.S. (2007). Transverse energy flows in vectorial fields of paraxial light beams, *Proc. of SPIE 2007,* V. 6729, 67290G

[50] Angelsky, O.V.; Yermolenko, S.B.; Zenkova, C.Yu. & Agelskaya, A.O. (2008). Polarization manifestations of correlation (intrinsic coherence) of optical fields, *Appl. Opt.*, V. 47, (2008), pp. 5492-5499

[51] Angelsky, O.V.; Zenkova, C.Yu.; Gorsky, M.P. & Gorodyns'ka, N.V. (2009). On the feasibility for estimating the degree of coherence of waves at near field, *Appl. Opt.*, V. 48, (2009), pp. 2784–2788

[52] Angelsky, O.V.; Gorsky, M.P.; Maksimyak, P.P.; Maksimyak, A.P.; Hanson, S.G. & Zenkova, C.Yu. (2011). Investigation of optical currents in coherent and partially coherent vector fields, *Opt. Expr.*, V. 19, (2011), pp. 660-672

[53] Turkevich, J.; Stevenson, P.C. & Hiller, J. (1951). A study of the nucleation and growth processes in the synthesis of colloidal gold, *J. Discuss. Faraday Soc.*, V. 11, (1951), pp. 55-75

[54] Angelsky, O.V.; Hanson, S.G.; Maksimyak, P.P.; Maksimyak, A.P. & Negrych, A.L. (2008). Experimental demonstration of singular-optical colouring of regularly scattered white light, *J. Europ. Opt. Soc. Rap. Public.*, V. 3, (2008), 08029

[55] Angelsky, O.V.; Hanson, S.G.; Maksimyak, A.P. & Maksimyak, P.P. (2005). Feasibilities of interferometric and chromascopic techniques in study of phase singularities, *Appl. Opt.*, V. 44, (2005), pp. 5091-5100

[56] Angelsky, O.V.; Maksimyak, A.P.; Maksimyak, P.P. & Hanson, S.G. (2005). Interference diagnostics of white-light vortices, *Opt. Expr.*, V. 13, (2005), pp. 8179-8183

[57] Angelsky, O.V.; Hanson, S.G.; Maksimyak, A.P. & Maksimyak, P.P. (2005). On the feasibility for determining the amplitude zeroes in polychromatic fields, *Opt. Expr.*, V. 13, (2005), pp. 4396-4405

[58] Angelsky, O.V.; Hanson, S.G.; Maksimyak, A.P. & Maksimyak, P.P. (2006). Optical correlation diagnostics of rough surfaces with large surface inhomogeneities, *Opt. Expr.*, V. 14, (2006), pp. 7299-7311

[59] Angelsky, O.V.; Polyanskii, P.V. & Hanson, S.G. (2006). Singular-optical coloring of regularly scattered white light, *Opt. Expr.*, V. 14, (2006), pp. 7579-7586
[60] Angelsky, O.V.; Bogatyryova, H.V. & Polyanskii, P.V. (2008). Interference coloring of regularly scattered white light, *Opt. Appl.*, V. 38, (2008), pp. 431-444
[61] Felde, Ch.V.; Chernyshov, A.A.; Bogatyryova, H.V.; Polyanskii, P.V. & Soskin, M.S. (2008). Polarization singularities in partially coherent combined beams, *JETP Lett.*, V. 88, (2008), pp. 418-422
[62] Chernyshov, A.A.; Felde, K.V.; Bogatyreva, G.V.; Polyanskii, P.V. & Soskin, M.S. (2009). Vector singularities of superposition of mutually incoherent orthogonaly polarized beams, *Opt. Spectr.*, V. 107, (2009), pp. 645-650
[63] Chernyshov, A.A.; Felde, Ch.V.; Bogatyryova, H.V.; Polyanskii, P.V. & Soskin, M.S. (2009). Vector singularities of the combined beams assembled from mutually incoherent orthogonally polarized components, *J. Opt. A: Pure Appl. Opt.*, V. 11, (2009), 094010
[64] Polyanskii, P.V.; Felde, Ch.V. & Chernyshov, A.A. (2010). Polarization degree singularities, *Proc. of SPIE 2010*, V. 7388, 7388OA
[65] Soskin, M.S. & Polyanskii, P.V. (2010). New polarization singularities of partially coherent light beams, *Proc. of SPIE 2010,* V. 7613,7613OG
[66] Polyanskii, P.V. & Bogatiryova, G.V. (2001). EDW: edge diffraction wave, edge dislocation wave, or whether *tertio est datur*?, *Proc. of SPIE*, V. 4607, pp. 109-124
[67] Bogatyryova, G.V.; Felde, Ch.V.; Polyanskii, P.V.; Ponomarenko, S.A.; Soskin, M.S. & Wolf, E. (2003). Partially coherent vortex beams with a separable phase, *Opt. Lett.*, V. 28, (2003), pp. 878-880
[68] Soskin, M.S.; Polyanskii, P.V., & Arkhelyuk, O.O. (2004). Computer-synthesized hologram-based rainbow optical vortices, *New J. Phys.*, V. 6, (2004), p. 196
[69] Berry, M.V., & Dennis, M.R. (2004). Quantum cores of optical phase singularities, *J. Opt. A.: Pure Appl. Opt.*, V. 6, (2004), p.178
[70] Freund, I.; Mokhun, A.I.; Soskin, M.S.; Angelsky, O.V. & Mokhun, I.I. (2002). Stokes singularity relations, *Opt. Lett.*, V. 27, (2002), pp. 545-547
[71] Angelsky, O.V.; Mokhun, I.I.; Mokhun, A.I. & Soskin, M.S. (2002). Interferometric methods in diagnostics of polarization singularities, *Phys. Rev. E.*, V. 65, (2002), 036602(5)
[72] Angelsky, O.V.; Mokhun, A.I.; Mokhun, I.I. & Soskin, M.S. (2002). The relationship between topological characteristics of component vortices and polarization singularities, *Opt. Commun.*, V. 207, (2002), pp. 57-65
[73] Ponomarenko, S.A. (2001). A class of partially coherent vortex beams carrying optical vortices, *J. Opt. Soc. Am. A*, V. 18, (2001), 150-156
[74] Gbur, G. & Visser, T.D. (2003). Coherence vortices in partially coherent beams, *Opt. Commun.*, V. 222, (2003), pp. 117-125
[75] Schouten, H.F.; Gbur, G.; Visser, T.D. & Wolf, E. (2003). Phase singularities of the coherence functions in Young's interference pattern, *Opt. Lett.*, V. 28, (2003), pp.968-970
[76] Swartzlander, G.A. Jr. & Schmit, J. (2004). Temporal correlation vortices and topological dispersion, *Phys. Rev. Lett.*, V. 93, (2004), 093901
[77] Gbur, G.; Visser, T.D. & Wolf, E. (2002). Anomalous behavior of spectra near phase singularities of focused waves, *Phys. Rev. Lett.*, V. 88, (2002), 013901

[78] Popescu, G. & Dogariu , A. (2002). Spectral anomalies at wave-front dislocations, *Phys. Rev. Lett.*, V. 88, (2002), 183902
[79] Berry, M.V. (2002). Colored phase singularities, *New J. Phys*, V. 4, (2002), p. 66
[80] Berry, M.V. (2002). Exploring the colors of dark light, *New J. Phys*., V. 4, (2002), p. 74
[81] Volyar, A.V. & Fadeyeva, T.A. (2003). Generation of singular beams in uniaxial crystals, *Opt. Spectr*., V. 94, (2003), pp. 260-270
[82] Egorov, Yu.A.; Fadeyeva, T.A. & Volyar, A.V. (2004). The fine structure of singular beams in crystals: colors and polarization, *J. Opt. A.: Pure Appl. Opt*., V. 6, (2004), p. 217
[83] Azzam, R.M.A. & Bashara, N.M. (1977). *Ellipsometry and Polarized Light,* North-Holland, Amsterdam
[84] Shurcliff, W.A. (1962). *Polarized Light: Production and Use,* Harvard Univ. Press, Cambridge, Massachusetts
[85] Lang, M.J. & Block, S. M. (2003). Resource Letter: LBOT-1: Laser-based optical tweezers, *Am. J. Phys.*, V. 71, (2003), pp. 201-205
[86] Allen, L.; Padgett, M.J. & Babiker, M. (1999). The orbital angular momentum of light, In: *Progress in Optics,* Wolf, E., V. 39, (1999), pp. 292-372
[87] Mokhun, I.; Brandel, R. & Viktorovskaya, Ju. (2006). Angular momentum of electromagnetic field in areas of polarization singularities, *Ukr. J. Phys. Opt.*, V. 7, (2006), pp. 63– 73
[88] Berry, M.V. (1998). Paraxial beams of spinning light, *Proc. of SPIE 1998*, V.3487
[89] Allen, L. & Padgett, M.J. (2000). The Poynting vector in Laguerre-Gaussian beams and the interpretation of their angular momentum density, *Opt. Comm.*, V. 198, (2000), pp. 67–71
[90] Berry, M.V. (2005). Phase vortex spirals, *J. Phys. A*, V. 38, (2005), pp. 745–751
[91] Mokhun, I.; Khrobatin, R.; Mokhun, A. & Viktorovskaya, Ju. (2007). The behavior of the Poynting vector in the area of elementary polarization singularities, *Opt. Appl*., V. 37, (2007), pp. 261–277
[92] Shvartsman, N. & Freund, I. (1995). Speckle spots ride phase saddles side saddle, *Opt. Com*., V. 117, (1995), pp. 228-234
[93] Jarry, G.; Steimer, E.; Damaschini, V.; Epifanie, M.; Jurczak, M. & Kaiser, R. (1998). Coherence and polarization of light propagating through scattering media and biological tissues, *Appl. Opt*., V. 37, (1998), 7357
[94] De Boer, J.F.; Milner, T.E.; Ducros, M.G.; Srinivas, S.M. & Nelson, J.S. (2002). Polarization-sensitive optical coherence tomography, In: *Handbook of Optical Coherence Tomography*. Bouma B.E.; Tearney G.J., pp. 237-274, Marcel Dekker Inc.: New York
[95] Zimnyakov, D.A. & Tuchin V.V.(2002). Optical tomography of tissues, *Quantum Electronics*, V.32, (2002), pp. 849-867
[96] Fercher, A. F. (2003). Optical coherence tomography – principles and applications, *Rep. Prog. Phys*., V. 66, (2003), pp. 239-303.
[97] Ushenko, A.G. & Pishak, V.P. (2004). Laser Polarimetry of Biological Tissue. Principles and Applications, In: *Coherent-Domain Optical Methods. Biomedical Diagnostics, Environmental and Material Science,* Tuchin. V., p. 67, Kluwer Academic Publishers
[98] Gori, F.; Santarsiero, M.; Vicalvi, S.; Borghi, R. & Guattari, G. (1998). Beam coherence-polarization matrix, *Pure Appl. Opt*., V. 7, (1998), pp. 941-951

[99] Mujait, C. & Dogariu, A. (2004). Statistics of partially coherent beams: a numerical analysis, *J. Opt. Soc. Am. A*., V 21, No. 6, (2004), pp. 1000-1003

[100] Angelsky, O.V.; Ushenko, A.G. & Ushenko, Ye.G. (2005). Complex degree of mutual polarization of biological tissue coherent images for the diagnostics of their physiological state, *J Biomed Opt*., V. 10. No. 6, (2005), pp. 060502

[101] Everett, M.J.; Shoenenberger, K.; Colston, B.W. & Da Silva, L.B. (1998). Birefringence characterization of biological tissue by use of optical coherence tomography, Opt. Lett., V. 23, (1998), pp. 228-230

[102] Mujait, M. & Dogariu, A. (2003). Polarimetric and spectral changes in random electromagnetic fields, *Opt. Lett*., V. 28, (2003), pp. 2153-2155

[103] Angelsky, O.V.; Ushenko, A.G.; Ushenko, Yu.A.; Pishak, V.P. & Peresunko, A.P. (2010). Statistical, Correlation, and Topological Approaches in Diagnostics of the Structure and Physiological State of Birefringent Biological Tissues, In: *Handbook of Photonics for Biomedical Science*, Tuchin, V.V., pp. 21-67, USA: CRC Press

[104] De Boer, J.F.; Milner, T.E.;. Van Gemert, M.J.C. & Nelson, J.S. (1997). Two-dimensional birefringence imaging in biological tissue by polarization-sensitive optical coherence tomography, *Opt. Lett*., V. 22, (1997), pp. 934-936

[105] De Boer, J.F.; Milner, T.E. &. Nelson, J.S. (1999). Determination of the depth-resolved Stokes parameters of light backscattered from turbid media by use of polarization-sensitive optical coherence tomography, *Opt. Lett*., V. 24, (1999), pp. 300-302

[106] Saxer, C.E.; de Boer, J.F.; Park, B.H.; Zhao, Y.; Chen, Z. & Nelson, J. S. (2000). High-speed fiber based polarization-sensitive optical coherence tomography of in vivo human skin, *Opt. Lett*., V. 25, (2000), pp. 1355-1357

[107] De Boer, J.F. & Milner, T.E. (2002). Review of polarization sensitive optical coherence tomography and Stokes vector determination, *J. Biomed. Opt*., V. 7, (2002), pp. 359-371

[108] Wolf, E. (1959). Coherence properties of partially polarized electromagnetic radiation, *Nuovo Cimento*., V. 13, (1959), pp. 1165–1181

[109] Mujait, M.; Dogariu, A. & Agarwal, G.S. (2004). Correlation matrix of a completely polarized, statistically stationary electromagnetic field , *Opt. Lett*., V. 29, (2004), pp. 1539-1541

[110] Korotkova, O. & Wolf, E. (2004). Spectral degree of coherence of a random three-dimensional electromagnetic field, *J. Opt. Soc. Am. A*., V. 21, No.10, (2004), pp. 2382-2385

[111] Angelsky, O.V.; Demianovsky, G. V.; Ushenko, A. G.; Burkovets, D. N. & Ushenko, Yu. A. (2004). Wavelet analysis of two-dimensional birefringence images of architectonics in biotissues for diagnosing pathological changes, *J. Biomed. Opt*., V. 9, (2004), pp. 679-690

[112] Angelsky, O.V.; Tomka, Yu.Ya.; Ushenko, A.G.; Ushenko, Ye.G. & Ushenko, Yu.A. (2005). Investigation of 2D Mueller matrix structure of biological tissues for pre-clinical diagnostics of their pathological states, *Journal of Physics D: Applied Physics,* V. 38(23), (2005), pp. 4227-4235

[113] Cowin, S.C. (2000). How is a tissue built?, *J. Biomed. Eng*., V. 122, (2000), pp. 553-568

[114] Ushenko, A.G.; Pishak, V.P.;. Yermolenko, S.B.; Pishak, O.V. & Burkovets, D.N. (1997). Laser measurements of crystal optical properties of blood-formed elements, *Proc. of SPIE 1997*, V. 3317, pp. 425-433

[115] Ushenko, A.G. (1999). Laser diagnostics of biofractals, *Quantum Electronics*, V. 29(12), (1999), pp. 1078–1084

[116] Angelsky, O.; Burkovets, D.; Pishak, V.; Ushenko, Yu. & Pishak, O. (2000). Polarization-correlation investigations of biotissue multifractal structures and their pathological changes diagnostics, *Laser Physics*., V. 10, №5, (2000), pp. 1136-1142

[117] Gori, F. (1998). Matrix treatment for partially polarized, partially coherent beams, *Opt. Lett*., V. 23, (1998), pp. 241-243

[118] Ushenko, Ye. G. (2005). Complex Degree of Mutual Polarization of Biotissue's Speckle-Images, *Ukr. J. Phys Opt*., V. 6, No. 3, (2005), pp. 104-113

[119] Ushenko, A.G. (1995). Polarization structure of laser scattering fields, Optical Engineering, V. 34(4), (1995), pp. 1088-1093

[120] Ushenko, A.G. (2000). Polarization Structure of Biospeckles and the Depolarization of Laser Radiation, Optics and Spectroscopy, V. 89(4), (2000), pp. 597-601

[121] Ushenko, A.G.; Ermolenko, S.B.; Burkovets, D.N. & Ushenko, Yu.A. (1999). Polarization Microstructure of Laser Radiation Scattered by Optically Active Biotissues, *Optics and Spectroscopy*, V. 87(3), (1999), pp. 434-439

Modern Metrology Concerns

Edited by Dr. Luigi Cocco

ISBN 978-953-51-0584-8
Hard cover, 458 pages
Publisher InTech
Published online 16, May, 2012
Published in print edition May, 2012

"What are the recent developments in the field of Metrology?" International leading experts answer this question providing both state of the art presentation and a road map to the future of measurement science. The book is organized in six sections according to the areas of expertise, namely: Introduction; Length, Distance and Surface; Voltage, Current and Frequency; Optics; Time and Relativity; Biology and Medicine. Theoretical basis and applications are explained in accurate and comprehensive manner, providing a valuable reference to researchers and professionals.

How to reference

In order to correctly reference this scholarly work, feel free to copy and paste the following:

O. V. Angelsky, P. V. Polyanskii, I. I. Mokhun, C. Yu. Zenkova, H. V. Bogatyryova, Ch. V. Felde, V. T. Bachinskiy, T. M. Boichuk and A. G. Ushenko (2012). Optical Measurements: Polarization and Coherence of Light Fields, Modern Metrology Concerns, Dr. Luigi Cocco (Ed.), ISBN: 978-953-51-0584-8, InTech, Available from: http://www.intechopen.com/books/modern-metrology-concerns/the-state-of-the-art-ande-prospects-of-metrology

INTECH
open science | open minds

InTech Europe
University Campus STeP Ri
Slavka Krautzeka 83/A
51000 Rijeka, Croatia
Phone: +385 (51) 770 447
Fax: +385 (51) 686 166
www.intechopen.com

InTech China
Unit 405, Office Block, Hotel Equatorial Shanghai
No.65, Yan An Road (West), Shanghai, 200040, China
中国上海市延安西路65号上海国际贵都大饭店办公楼405单元
Phone: +86-21-62489820
Fax: +86-21-62489821

IntechOpen